NIS-ALT

NIS-P

James E. Hansen
Inst. for Space Studies
New York, N.Y.
unnumbered report
September, 1972

INFORMATION CONTAINED IN THE INTENSITY AND POLARIZATION OF SCATTERED SUNLIGHT

1. DESCRIPTION OF RADIATION
   a. Intensity
   b. Linear Polarization
   c. Circular Polarization
2. EFFECT OF PARTICLE SIZE
   a. Geometrical Optics
   b. Rayleigh Scattering
   c. Intermediate Particle Sizes
3. SINGLE SCATTERING
   a. Ray Optics vs. Mie Scattering
   b. Effect of Size Distribution
   c. Effect of Refractive Index
   d. Nonspherical Particles
4. MULTIPLE SCATTERING
5. APPLICATION TO EARTH CLOUDS
   a. Potential Cloud Information
   b. Theoretical Computations in the Infrared
   c. Cloud Observations
6. APPLICATION TO VENUS
7. POTENTIAL APPLICATIONS ON MJS
   a. Cloud Heights and Macrostructure
   b. Particle Sizes
   c. Particle Microstructure

INFORMATION CONTAINED IN THE INTENSITY AND POLARIZATION OF SCATTERED SUNLIGHT

1. DESCRIPTION OF RADIATION

The purpose of this appendix is to discuss how scattered sunlight depends on the nature of the scattering material. Much of the information which we would like to obtain on planets, satellites, the rings of Saturn and interplanetary particles is contained in scattered radiation which can be measured with remote passive techniques. An understanding of the ways in which the characteristics of the radiation depend on the properties of the observed bodies is essential if we are to make an optimum choice for the type of measurements, the wavelength intervals and the geometry of observation. Such an understanding is also required in order that we may know the degree of certainty which can be attached to information obtained from scattered light.

All passive methods of remote sensing rely on measurements of the intensity of radiation striking some detector. An instrument for optically transforming the received radiation may precede the detector. At each wavelength the radiation can be completely defined as far as practical analysis is concerned by four parameters; these parameters thus contain the total available information in the received radiation. Although we may choose from a variety of ways to mathematically represent radiation, the most useful physical description is in terms of the intensity, the linear polarization (its degree and direction) and the circular polarization. All of these quantities can be measured as a function of wavelength, the scattering geometry (the directions of the observer and of the sun) and location on the planet or other observed medium.

The intensity is the quantity most commonly measured, and it can be effectively used in a variety of ways. Observations of absorption lines at high spectral resolution yield information on the gaseous composition of an atmosphere and on the temperature and pressure distributions; however, the accuracy with which quantitative information can be obtained depends on how much independent knowledge of the atmospheric structure is available, particularly on the nature and distribution of scatterers. Broad-band measurements of the intensity of light scattered by planetary atmospheres and surfaces are also commonly made; although these observations are not often subject to unique interpretations they do help to limit the possibilities for the composition of the scatterers. Imaging devices yield the spatial variation of the intensity of scattered sunlight; this can provide information on the structure of clouds or of a planetary surface.

The linear polarization is less commonly measured than the intensity, perhaps partly because it requires some additional instrumentation, partly because it is less familiar to us* and partly because less work has been done in interpreting polarizations than in interpreting intensities. However, the linear polarization has the major advantage that it can be obtained from a relative measurement with a higher accuracy (~ 0.2%) than that with which the intensity can be measured. It has also been demonstrated with laboratory and theoretical work that errors of measurement can be kept much smaller than the characteristic features in the linear polarization, and that the features can be simply interpreted to yield information on the scattering material.

The circularly polarized component of sunlight reflected by planets has been measured and found to be very small (Kemp, et al., 1971). The characteristics of the circular polarization are in agreement with theoretical expectations (Hansen, 1971a); however, in many common situations the circular polarization arises only via the process of multiple scattering which tends to garble potential information on the scattering materials. This latter fact together with the small value of the circular polarization and the fact that only a small amount of theoretical work has been done on it indicates that measurements of the circular polarization of scattered sunlight are not yet a candidate for spacecraft observations. Therefore in the following parts of this appendix we will be concerned primarily with the intensity and linear polarization.

---

*Although the eyes of humans are not very sensitive to polarization, those of many animals and insects are. This allows them to use the polarization of skylight as a very effective means of navigation.

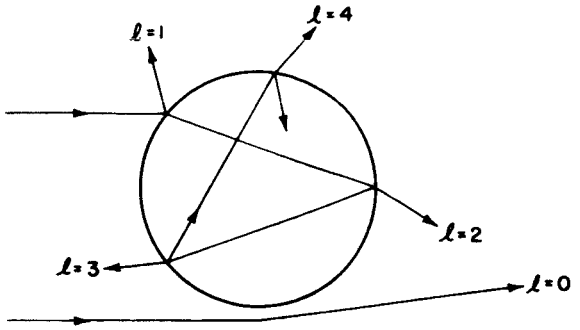

TERMINOLOGY FOR CONTRIBUTIONS TO SCATTERED LIGHT:

ℓ

0 - DIFFRACTION

1 - EXTERNAL REFLECTION

2 - TWICE REFRACTED RAYS

3 - ONE INTERNAL REFLECTION

4 - TWO INTERNAL REFLECTIONS

PHASE FUNCTION:

$$P(\alpha) = \sum_{\ell=0}^{\infty} P_\ell(\alpha)$$

$$\int_{4\pi} P$$

ℓ	$n_r = 1.33$	$n_r = 2.00$
0	.500	.500
1	.033	.081
2	.442	.364
3	.020	.043
4	.003	.008
>4	.002	.004

Fig. 1. Paths of light rays scattered by a sphere according to geometrical optics and diffraction. P is the phase function and α the scattering angle. The table on the right gives the fraction of the total scattered light contributed by each value of ℓ for nonabsorbing spheres with refractive indices 1.33 and 2.0.

2. EFFECT OF PARTICLE SIZE

The manner in which scattered light depends on the nature (size, shape and optical properties) of the scattering material can be understood qualitatively, and in many cases quantitatively, in terms of simple physical models. These models are most useful for cases in which light is scattered <u>independently</u> by the different particles composing a given medium, i.e. for situations in which the particles are sufficiently far from each other. This is the case for all planetary atmospheres (both for gas molecules and haze and cloud particles), for the interplanetary medium and probably for the rings of Saturn.

Scattering by a planetary surface involves the additional complication that neighboring particles scatter coherently, so the intensities scattered by the various parts of the surface can not be added without regard to phase. Although most of the concepts that we will discuss are valid for particles on a planetary surface, as well as for independently scattering particles, useful methods for detailed theoretical modeling of light scattering by a planetary surface have not been developed. Therefore the interpretation of observations of planetary surfaces must rely in large part on comparisons to laboratory data, and the conclusions which can be derived are not as quantitative as in the case of scattering by independent particles.

<u>Geometrical Optics</u>. For large particles the scattering can be understood in terms of the concepts of geometrical optics. In this case the light incident on a particle may be thought of as consisting of separate rays of light which pursue independent paths. For a particle with a size at least several times the wavelength it is possible to distinguish rays striking various local regions on the particle's surface.

Fig. 1 illustrates the terminology used for the different contributions to the light scattered by a large particle. The division of rays into these different components is valid for all particle shapes, though the fraction of light which goes into the different components has some dependence on particle shape.

The light rays which miss the particle ($\ell = 0$) are partially diffracted into the geometrical shadow of the particle. The amount of diffracted light is equal to the amount striking the particle, and hence for nonabsorbing particles it constitutes exactly half of the scattered light. This fraction is independent of the particle shape and refractive index. The angular distribution of the diffracted light does depend on the particle shape. However, the dependence is slight if the particles are randomly oriented and it can be easily computed for any particle shape. The polarization of diffracted light is zero in the limit of large particles, except for the fact that diffracted light can optically interfere with light which is reflected ($\ell = 1$) and transmitted ($\ell = 2$) by the particle (see Section 3).

The intensity and polarization of the light reflected from the outside of the particle ($\ell = 1$) may be computed from Fresnel's equations. For a transparent sphere the externally reflected light makes up only a few percent of the total scattered light, though the fraction

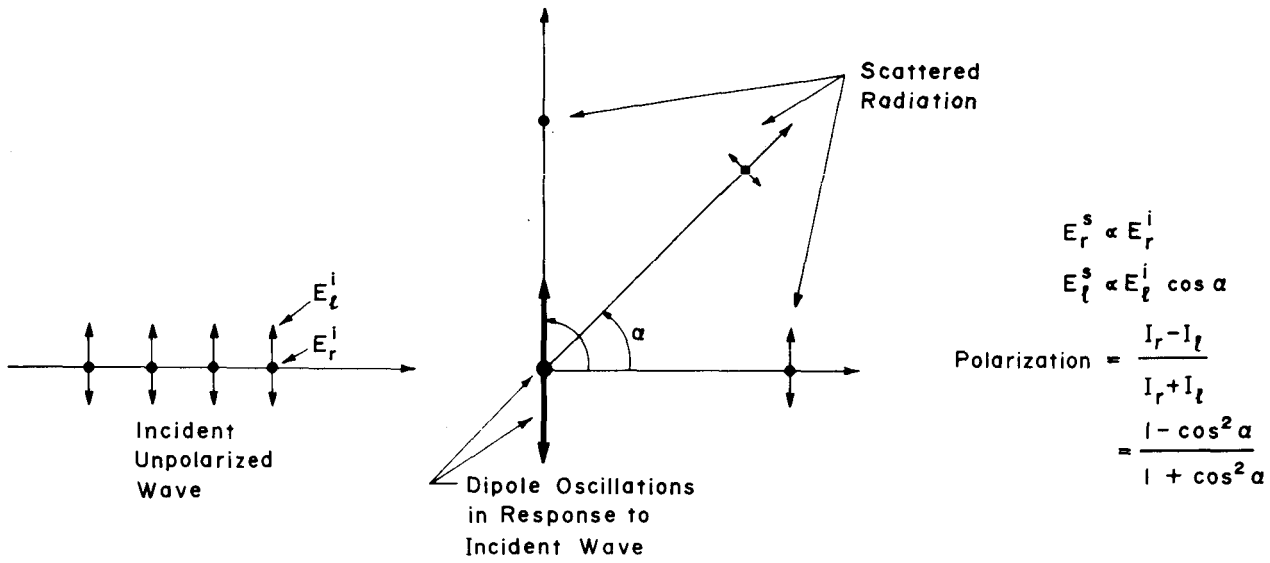

Fig. 2. Schematic representation of Rayleigh scattering. The unpolarized wave incident from the left can be represented by two linearly polarized waves vibrating at right angles to each other with equal electric field strengths ($E_\ell^i = E_r^i$) and a random phase relationship. The electrons in a small particle will oscillate in response to the electric components of the incident wave, their motion being equivalent to two oscillating dipoles whose axes are represented by the heavy arrow and dot. The dipoles, which do not radiate in their direction of action, give rise to the indicated scattered fields and intensities.

increases as the refractive index increases. For randomly oriented convex nonspherical particles the external reflection makes up exactly the same fraction of the scattered light as it does for spheres, and the angular distribution and polarization of the reflected light are the same as they are for spherical particles.

The rays which are refracted twice without any internal reflections ($\ell = 2$) make up a large fraction of the scattered light for transparent or partially transparent spheres. This conclusion holds for nonspherical particles also, although the exact fraction does depend on the particle shape even if the particles are randomly oriented.

The light which is internally reflected in particles represents only a few percent of the scattered light. The angular distribution and polarization for these rays can be computed for any particle shape using Snell's law and the Fresnel reflection coefficients. For spheres the $\ell = 3$ and $\ell = 4$ terms give rise to the primary and secondary rainbows. The intensity of higher terms is negligible.

In Section 3 computations for scattering by spheres are made using geometrical optics and the results are compared to exact computations for finite spheres.

Rayleigh Scattering. The case of small particles provides the simplest scattering behavior, Rayleigh scattering. The requirement for Rayleigh scattering is that the particle size be much less than the wavelength both inside and outside of the particle. In this case the incident electromagnetic fields are uniform throughout the particle, which thus oscillates as a simple dipole in response to the incident radiation (Fig. 2).

The strong polarization for Rayleigh scattering, its simple dependence on scattering angle and its characteristic wavelength dependence (cross-section or optical thickness $\propto \lambda^{-4}$) provide sure means for separating scattering due to Rayleigh particles from that due to large particles.

Intermediate particle sizes. The limiting cases of geometrical optics and Rayleigh scattering are sufficient to describe most of the characteristics of light scattered by particles of all sizes. This is illustrated in Fig. 3 which shows the intensity and polarization for single scattering by a size distribution of spheres with a real refractive index $n_r = 1.33$. These are contour diagrams of the intensity and polarization as a

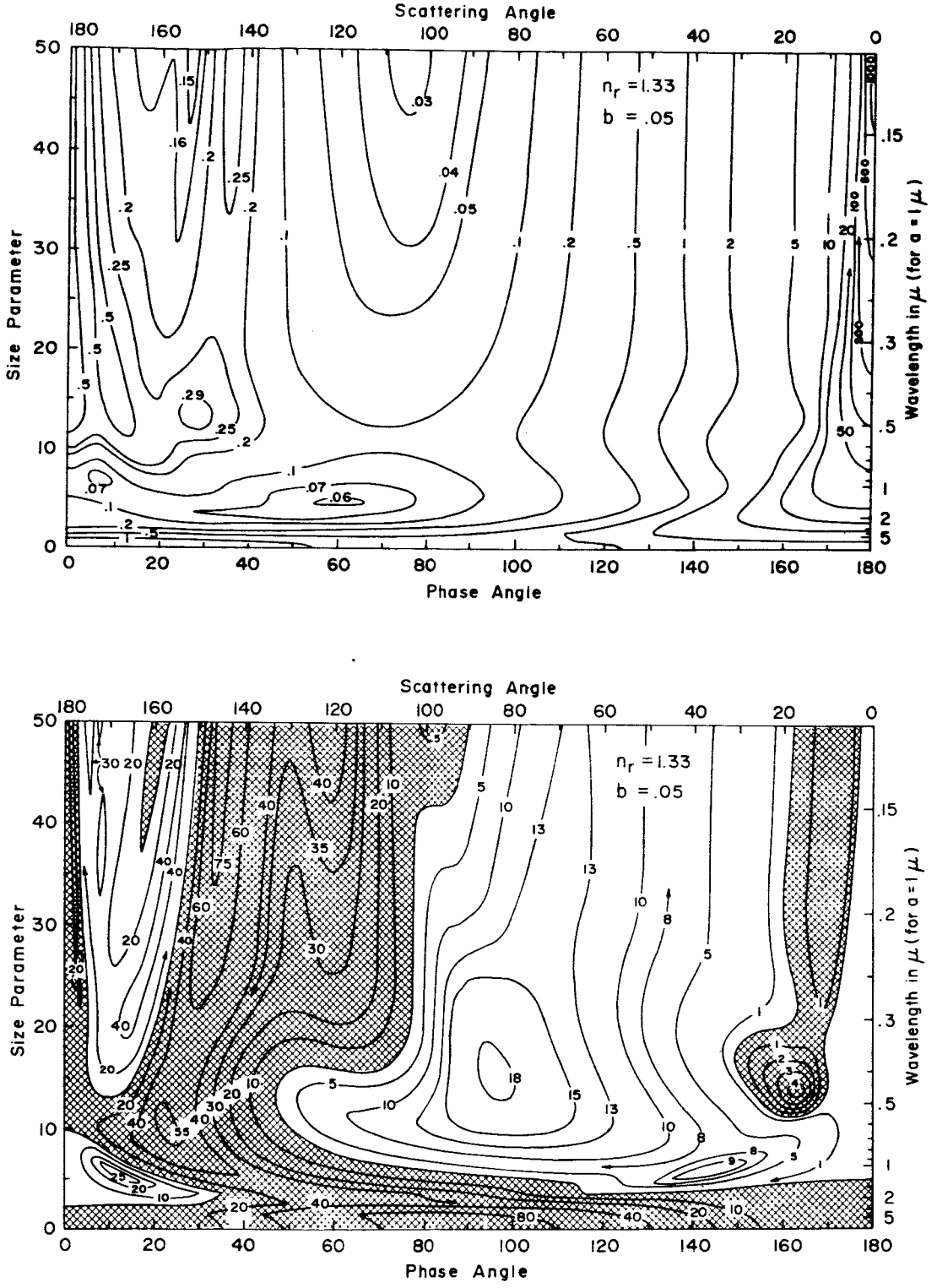

Fig. 3. Lower figure: contour diagram of the percent polarization for single scattering of unpolarized light by a size distribution of spheres with refractive index 1.33. The shaded areas indicate positive polarization ($I_r > I_\ell$) and the unshaded indicate negative values. The size parameter is $2\pi a/\lambda$. a is the effective mean radius and b the effective variance for the size distribution, for which the particular form was $n(r) \propto r^{(1-3b)/b}\, e^{-r/(ab)}$. Upper figure: the same as below, except that the contours are for the phase function (normalized intensity.)

function of the scattering angle, α, (or the phase angle, $180^\circ - \alpha$) and as a function of the mean size parameter for the distribution, $2\pi a/\lambda$, where a is the mean effective particle size. In Sec. 3 it is illustrated that the scattering by a size distribution can be accurately defined by the mean size, a, and variance, b, of the distribution, i.e., the higher moments of the distribution are negligible in most cases.

For size parameters near zero Rayleigh scattering occurs with its strong characteristic polarization. For the largest size parameters the features are essentially those of geometrical optics: the primary rainbow at a scattering angle $\alpha \sim 145^\circ$, the second rainbow for $\alpha \sim 120^\circ$ (which is noticable in the polarization for $x < 50$, but not in the intensity) and the negatively polarized twice refracted rays for $\alpha \lesssim 90^\circ$. The characteristics of all the features are discussed in Section 3.

As the size parameter decreases the features of geometrical optics become increasingly blurred until they are essentially lost for size parameters $x \lesssim 15$. This is as expected since $x = 15$ corresponds to a ratio of particle diameter to wavelength of ~5. Between $x \sim 15$ and the region of dipole (Rayleigh) scattering the results can be understood in terms of radiation due to higher multipole moments and surface waves. The manners in which these features depend on the refractive index and size distribution are illustrated and discussed in Section 3.

3. SINGLE SCATTERING

The properties of radiation scattered by isotropic homogeneous spheres can be obtained exactly from classical electromagnetic theory. The results for a single sphere depend on the index of refraction of the sphere relative to the surrounding medium [$n_c = n_r - i n_i$, where $i = (-1)^{\frac{1}{2}}$] and upon the ratio of the radius of the sphere to the wavelength of the incident radiation ($x = 2\pi r/\lambda$, where r is the particle radius and λ the wavelength). For these special particles the properties of radiation scattered in an arbitrary direction depend additionally only on the scattering angle, α, and are completely defined for any polarization state of the incident light by four functions of n_c, x and α. Using the notation of van de Hulst (1957) these four functions are

$$\begin{aligned} M_1(\alpha) &= |A_1(\alpha)|^2 \\ M_2(\alpha) &= |A_2(\alpha)|^2 \\ S_{21}(\alpha) &= |A_2(\alpha)A_1^*(\alpha) + A_1(\alpha)A_2^*(\alpha)|/2 \\ D_{21}(\alpha) &= |A_2(\alpha)A_1^*(\alpha) - A_1(\alpha)A_2^*(\alpha)|/2 \end{aligned} \tag{1}$$

where A_1 and A_2 are the complex scattering amplitudes, respectively perpendicular and parallel to the scattering plane, and the asterisk indicates the complex conjugate. For a size distribution (polydispersion) of independent scatterers the functions M_1, M_2, S_{21} and D_{21} are obtained by simple addition of those functions for all particles in the distribution; e.g.,

$$M_1(\alpha) = \int_{r_1}^{r_2} M_1(r,\alpha) n(r) dr \tag{2}$$

where $n(r)$ is the size distribution of particles and r_1 and r_2 correspond to the smallest and largest particles present.

For scattering problems the most practical representation of a beam of radiation is in terms of its Stokes parameters I, Q, U and V. I is the intensity of the beam, Q and U determine the linear polarization and V the circular polarization. The four functions in (1) uniquely define the scattered radiation in terms of the Stokes parameters of the incident radiation:

$$\begin{bmatrix} I \\ Q \\ U \\ V \end{bmatrix} = \begin{bmatrix} \frac{1}{2}(M_1+M_2) & \frac{1}{2}(M_2-M_1) & 0 & 0 \\ \frac{1}{2}(M_2-M_1) & \frac{1}{2}(M_1+M_2) & 0 & 0 \\ 0 & 0 & S_{21} & -D_{21} \\ 0 & 0 & D_{21} & S_{21} \end{bmatrix} \begin{bmatrix} I_o \\ Q_o \\ U_o \\ V_o \end{bmatrix} \tag{3}$$

It is convenient to further define a normalized phase matrix by means of

$$\begin{aligned} P^{11}(\alpha) &= c[M_1(\alpha)+M_2(\alpha)]/2 = P^{22}(\alpha) \\ P^{12}(\alpha) &= c[M_2(\alpha)-M_1(\alpha)]/2 = P^{21}(\alpha) \\ P^{33}(\alpha) &= c\, S_{21}(\alpha) = P^{44}(\alpha) \\ P^{43}(\alpha) &= c\, D_{21}(\alpha) = -P^{34}(\alpha) \end{aligned} \tag{4}$$

where the constant c is determined by the condition that

$$\int_{4\pi} P^{11}(\alpha) \frac{d\omega}{4\pi} = 1. \tag{5}$$

$P^{11}(\alpha)$ is the phase function, or the probability for scattering of unpolarized light at the scattering angle α. The degree of linear polarization is $-P^{21}(\alpha)/P^{11}(\alpha)$; for simplicity we will

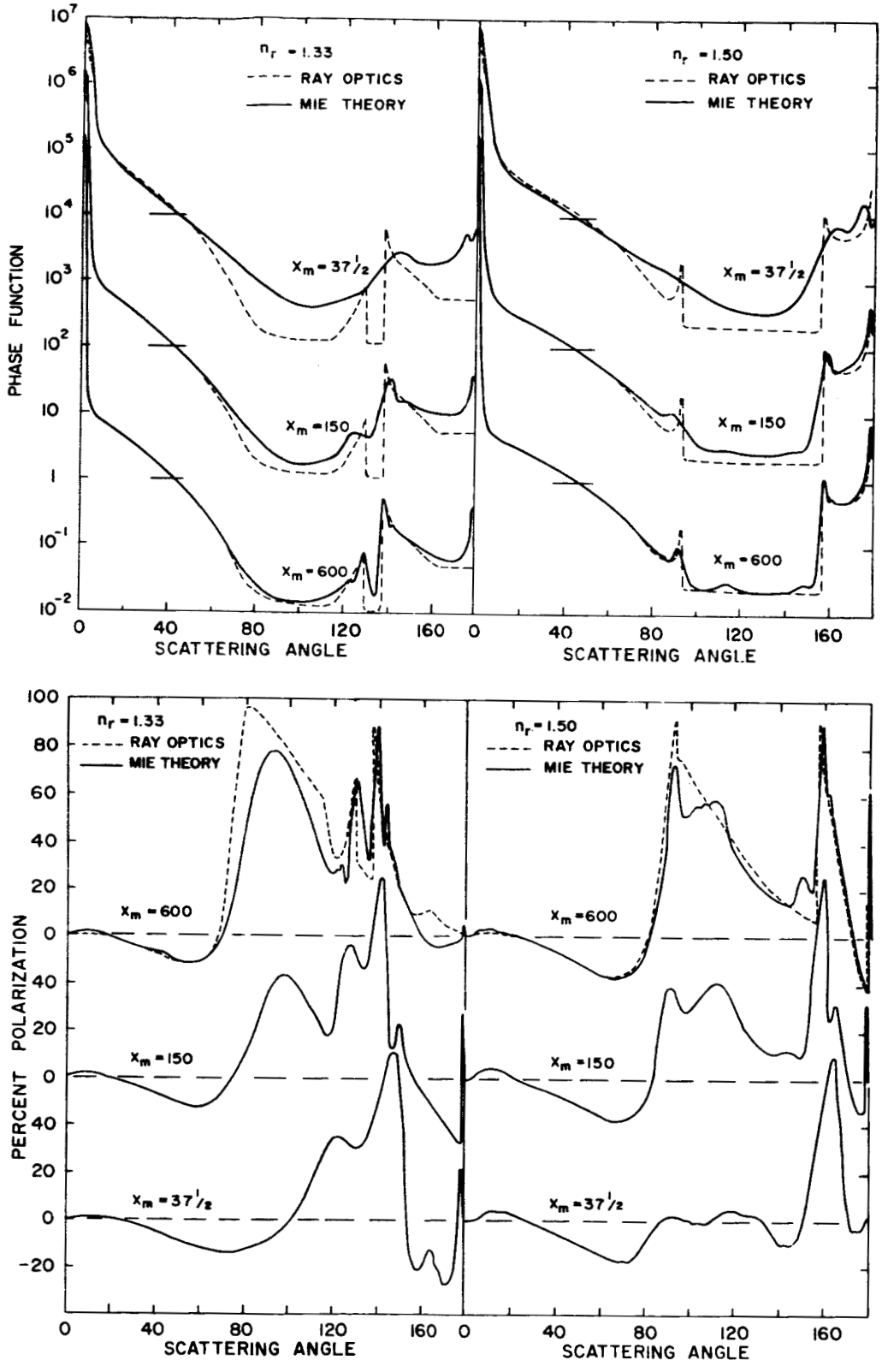

Fig. 4. Comparison of ray optics (geometrical optics and diffraction) and Mie theory for the percent polarization (upper figure) and phase function (lower figure) for scattering by spheres. The size distribution is $n(x) = x^{(1-3b)/b}\, e^{-x/x_m b}$ with $b = 1/9$. Results are shown for two refractive indices and three values of the effective mean size parameter, x_m. For the phase function the scale applies to the curves for $x_m = 600$, the other curves being successively displaced upwards by factors of 100.

sometimes refer to the latter as the 'degree of polarization' or just the 'polarization'.

Ray optics vs. Mie scattering. The ray-tracing approach of geometrical optics provides a physical explanation for most of the features which occur in the exact theory for scattering by spheres (Mie scattering). In the computations for geometrical optics illustrated in this section the contributions from rays undergoing diffraction ($\ell = 0$), reflection ($\ell = 1$), two refractions ($\ell = 2$), etc., are added without regard to phase. This is reasonable since in nature there is generally a size distribution of particles present which tends to wash out phase effects. We will, however, also consider the exceptions in which features due to interference between different rays are noticeable.

Fig. 4 illustrates the results of computations for both ray optics and Mie theory for two values of the refractive index, $n_r = 1.33$ and 1.50. These computations are for the particular size distribution

$$n(x) = x^6 \, e^{-9x/x_m} \qquad (6)$$

for three values of x_m, which is the effective mean size parameter for the distribution. For the purpose of comparing geometrical optics and Mie theory the shape of the size distribution is not essential.

In the curves for the phase function (intensity) the concentration of light near the scattering angle zero degrees represents the diffraction ($\ell = 0$) which is unpolarized. The contribution to the scattered light from $\ell = 1$ (external reflection) does not leave any apparent feature on the intensity, but it is strongly polarized and gives rise to the broad positive polarization feature for scattering angles in the range ~80 - 120 degrees. The energy contained in the $\ell = 2$ term (twice refracted rays) is concentrated in the forward scattering hemisphere and is negatively polarized, as follows from Fresnel's equations. The components involving internal reflections ($\ell \geq 3$) contain only a few percent of the scattered light, however, they give rise to observable optical phenomena which are useful for cloud particle identification.

'Rainbows' occur when the scattering angle α has an extremum as a function of the angle of incidence τ on the sphere. For example, for $n_r = 1.33$ as τ varies from 90° (central incidence) to 0° (grazing incidence), the scattering angle for rays internally reflected once, computed using Snell's law, decreases from 180° until it reaches ~138° (the angle of 'minimum deviation') from which it then increases again. The resulting concentration of energy at 138° and just greater angles is the primary rainbow.

The minor feature on the large scattering angle side of the primary rainbow is the first "supernumerary bow". This is not rendered by the geometrical optics computations because it is an interference feature. At these scattering angles there are $\ell = 3$ rays striking two different parts of the sphere but emerging with the same scattering angle; these rays optically interfere causing the supernumerary bows. The number and strength of the supernumerary bows depends on the shape of the size distribution, as discussed in the following subsection.

The enhanced scattering in the backscattering direction, $\alpha \sim 180°$, is the so-called glory. This is caused specifically by the spherical shape of the scatterers which serves to focus part of the scattered light at $\alpha \sim 180°$. More detailed discussions of the glory are given by van de Hulst (1957), Fahlen and Bryant (1968) and Liou and Hansen (1971).

Fig. 4 illustrates that there is a close quantitative agreement between ray optics and Mie theory only if the value of the mean size parameter is at least several hundred. However, most of the features of ray optics remain visible to a much smaller particle size, and indeed their variations with decreasing size parameter can be qualitatively understood in terms of the reduced validity of the localization of rays. The decreasing size causes the light in the individual features to be blurred over a wider range of angles than predicted by ray optics, and it usually affects higher values of ℓ first because they have a more detailed ray path within the sphere. Thus the secondary rainbow ($\ell = 4$) is quite smooth in the intensity for $x_m = 150$, and is lost for $x_m = 37\frac{1}{2}$, while the primary rainbow ($\ell = 3$) is still easily visible in both cases. Because of the asymmetric shape of the rainbows the smoothing due to a finite size parameter causes the peak of the rainbow to move slightly as the size parameter decreases.

Fig. 4 also illustrates that the

single scattering polarization, compared to the intensity, contains much stronger imprints of most of the features occuring in the scattered light. Furthermore, for the polarization these features remain visible to much smaller size parameters. These conclusions hold for the rainbows, the supernumerary bows, the glory, and the external reflection. The strength of these features for single scattering is a major reason why there is a high information content in polarization observations. The relative usefulness of polarization is further heightened by the fact that there is much less tendency for multiple scattering to wash out such features in the polarization than is the case for the intensity (Section 4).

Effect of size distribution. The characteristics of scattered light, its intensity and polarization in particular, depend upon the size distribution of particles as indicated by Equation (2). In the cases of interest we do not know this distribution, and indeed, it is one of the quantities which we would like to obtain from measurements of the scattered light. Since there are an infinite number of possible size distributions some authors have been uncertain as to how much unambiguous information can be extracted from scattered light. Actually the situation is much brighter than it may appear at first glance. The scattering properties of most physically plausible size distributions depend significantly on only a small number of characteristics of the distribution, e.g., on a measure of the average particle size and the width of the distribution. While it is thus not feasible to obtain the exact shape of the size distribution from scattered light it is possible to extract the major characteristics of the size distribution, and, as a consequence, it is also possible to obtain other properties of the scatterers.

Clearly the first parameter describing a size distribution should be some measure of the mean size. Since most particles scatter an amount of light at least in proportion to their area it is logical to define a mean effective radius for a size distribution as

$$\langle r \rangle_{eff} = \frac{\int_0^\infty r\ \pi r^2\ n(r)dr}{\int_0^\infty \pi r^2\ n(r)dr}, \qquad (7)$$

which differs from the simple mean radius only in the fact that the particle area is included as a weight factor multiplying n(r). For some properties of the scattered light $\langle r \rangle_{eff}$ is by itself an adequate specification of the size distribution. However, higher moments can sometimes be important, particularly for polarization. The effective variance is defined as

$$v_{eff} = \frac{\int_0^\infty (r-\langle r \rangle_{eff})^2 \pi r^2 n(r)dr}{\langle r \rangle_{eff}^2 \int_0^\infty \pi r^2 n(r)dr} \qquad (8)$$

where the factor $\langle r \rangle_{eff}^2$ in the denominator makes v_{eff} dimensionless and a relative measure. Additional moments of the size distribution may be defined analogously, but there is little need of them in practice.

Different particle size distributions having the same values of $\langle r \rangle_{eff}$ and v_{eff} have similar scattering properties. Thus it is possible to use an analytic size

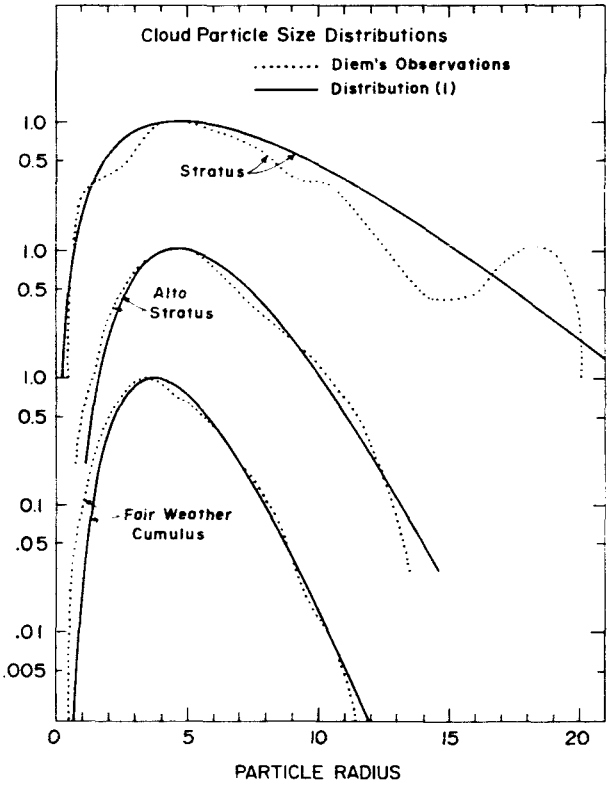

Fig. 5. Comparison of measured cloud particle size distribution (Diem, 1948) to the analytical size distribution (9), $n(r) \propto r^{(1-3b)/b}\ e^{-r/(ab)}$. a and b are the effective mean radius and the effective variance for the distributions.

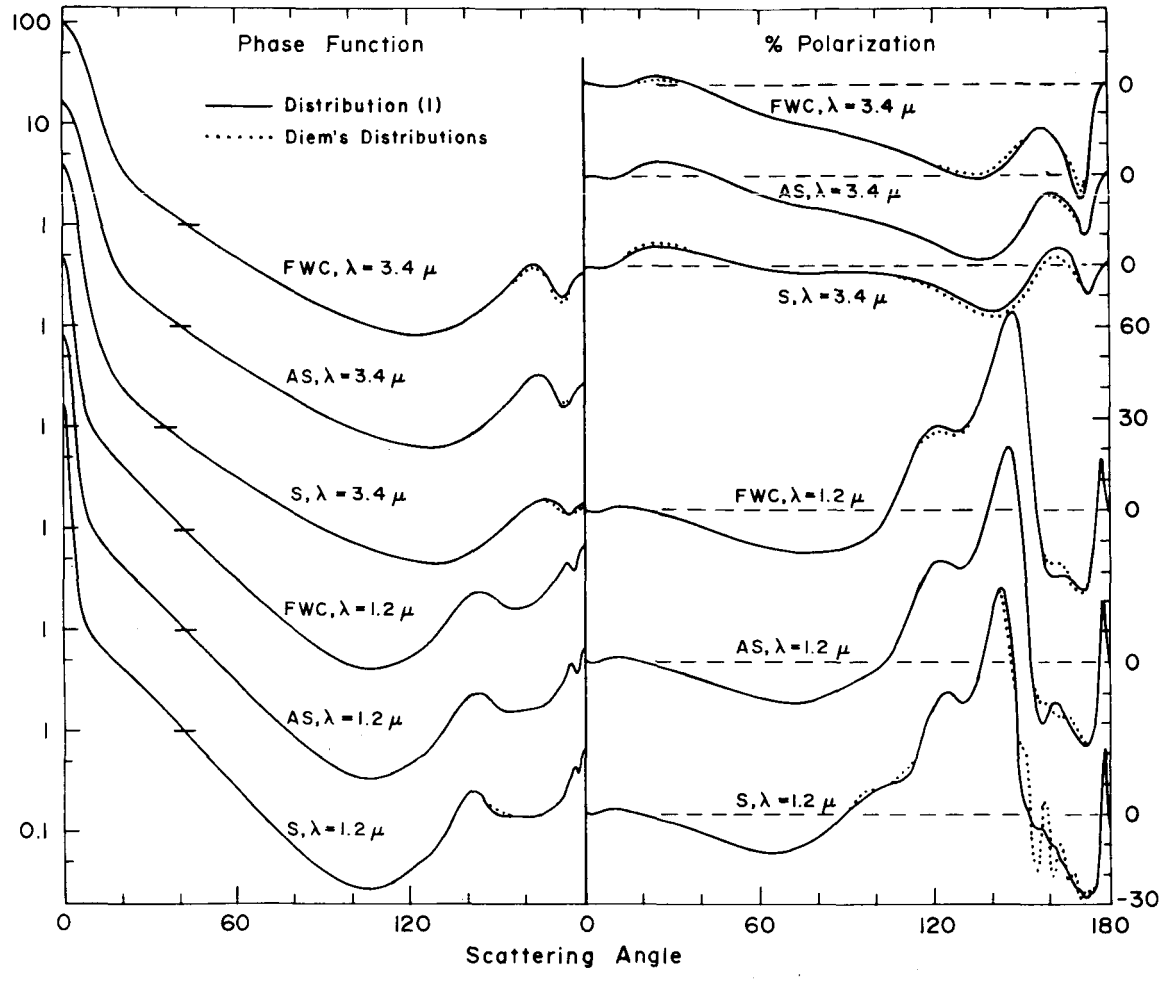

Fig. 6. Comparison of the phase function and percent polarization for single scattering by spheres for the size distribution shown in Fig. 5. FWC, AS and S represent fair weather cumulus, altostratus and stratus, respectively. The phase functions are displaced with the dashed lines indicating zero polarization.

distribution to represent a natural distribution. A particularly convenient analytic distribution is

$$n(r) = \text{constant } r^{(1-3b)/b}\, e^{-r/(ab)} \qquad (9)$$

which has the property that

$$\left.\begin{aligned} a &= \langle r \rangle_{eff} \\ b &= v_{eff} \end{aligned}\right\} \qquad (10)$$

i.e., the two parameters in the distribution are equal to the physical parameters which characterize the scattering by the size distribution.

Fig. 5 shows some measured size distributions for terrestrial water clouds compared to the standard distribution (9) with a and b specified by (10). In Fig. 6 the phase function and percent polarization are plotted for both the observed and analytic distributions. The latter figure is a typical example of differences in the scattering which occur for distributions with the same $\langle r \rangle_{eff}$ and v_{eff}. The differences are largest for the stratus cloud in which the observed distribution is bimodal with each mode contributing approximately an equal amount to the scattered light. However, even in this case the only significant difference in the scattering is for $\alpha \sim 160^{\circ}$; this is a region of optical interference and hence the results are particularly sensitive to the shape of the size distribution.

Since two parameters are sufficient to adequately define most size distributions it is possible to illustrate in a

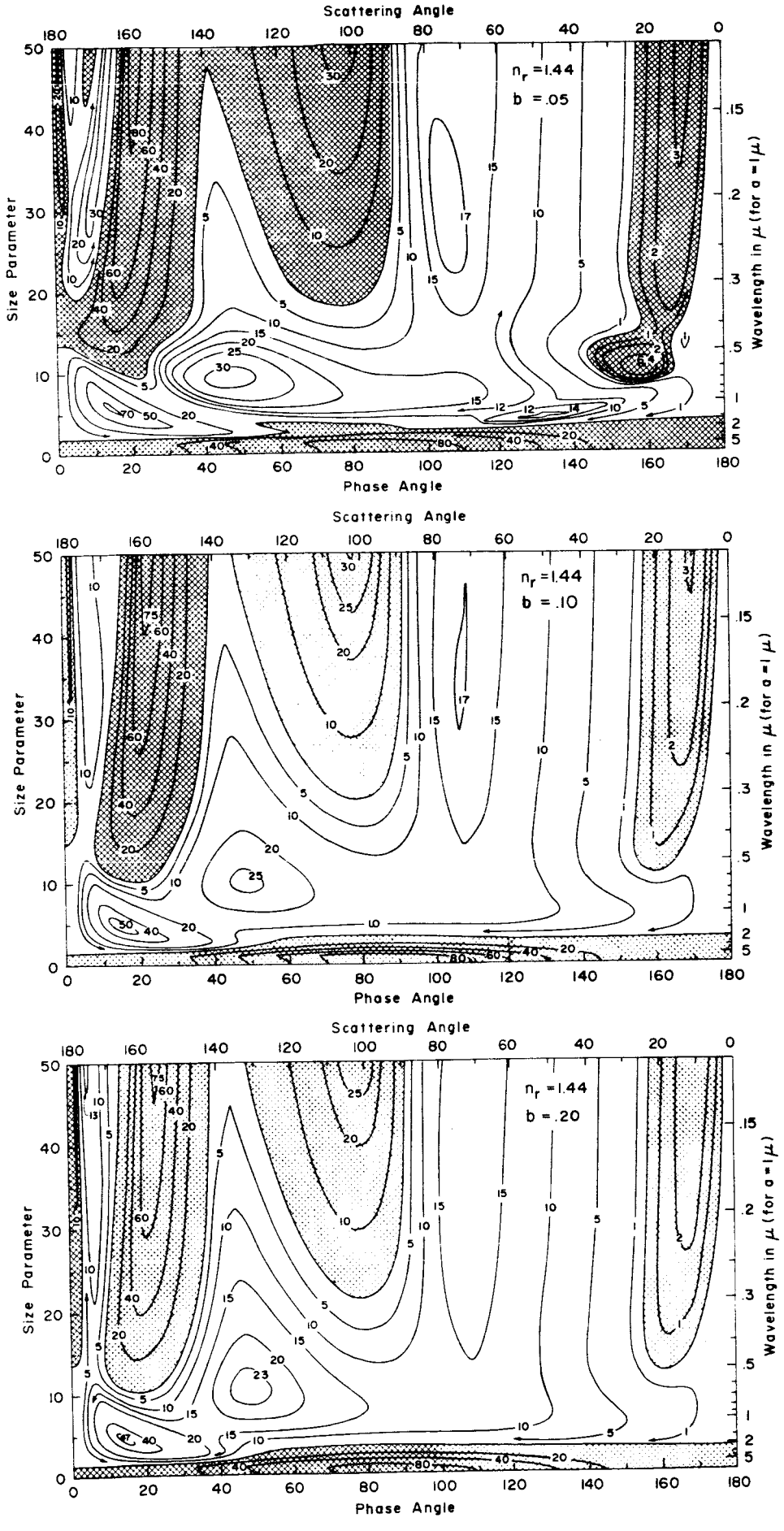

Fig. 7. Contour diagrams of the percent polarization for single scattering of unpolarized light by a size distribution of spheres.

The shaded areas indicate positive polarization ($I_r > I_l$) and the unshaded areas indicate negative values.

The size parameter is $2\pi a/\lambda$.

a is the effective mean radius and b is the effective variance for the size distribution, for which the particular form was $n(r) = r^{(1-3b)/b}\, e^{-r/ab}$.

A comparison of the three diagrams illustrates the effect of the width of the particle size distribution on the polarization.

small number of diagrams the effect of the size distribution on the scattered light. Fig. 7 shows contour diagrams of the polarization for a size distribution of spheres, as a function of scattering angle on the horizontal axis and as a function of mean effective size parameter, $2\pi a/\lambda$, on the vertical axis. These results are for the standard size distribution (9) with the three parts of the figure corresponding to different values of b, but all for the same refractive index, $n_r = 1.44$. The smallest value of b, .05, was selected to obtain a narrower distribution than is usually found for naturally occurring terrestrial cloud or haze particles. The other extreme value of b corresponds to a broad distribution by terrestrial standards (Sections 5 and 6). Note that the results for the broader distributions can be anticipated from those for the narrowest distribution, because they are essentially weighted averages along vertical lines.

It is useful to understand the features in these contour diagrams. The steep positive polarization ridge for scattering angles ~140 - 170° is of course the primary rainbow. As the size parameter decreases the rainbow becomes smoother and sinks into the negative polarization at $2\pi a/\lambda \sim 10$, where the concepts of geometrical optics have lost their validity. Broadening the size distribution smooths the rainbow at its small size parameter extremity, because only in that region is the rainbow significantly size dependent.

The positive feature for scattering angles ~90-130° is the second rainbow, which, as expected, is broader than the primary rainbow and disappears at a somewhat larger size parameter. The second rainbow also has little dependence on the width of the size distribution.

For scattering angles smaller than those of the second rainbow the polarization is essentially that of the twice refracted rays ($\ell=2$). However for $\alpha \sim 5\text{-}25°$ the external reflection ($\ell=1$) wins out over $\ell=2$ and gives rise to the positive polarization peninsula. This peninsula is connected to an island at $2\pi a/\lambda \sim 10$ for the case of the narrow distribution (b=.05). Obviously this island must be washed away for a broad distribution, and this is demonstrated in Fig. 7. This particular feature is due to optical interference between rays passing through the particles and those passing outside of it. Van de Hulst (1957) refers to this interference as 'anomalous diffraction'. This feature can be observed in the polarization of sunlight reflected by Venus and it has been mapped in detail for Venus (Section 6).

For the smallest sizes the positive polarization is Rayleigh scattering or dipole radiation (Section 2b). The scattered radiation field can in general be expanded in a series in which the successive terms correspond to the radiation arising from the different multipole moments induced in the particle by the incident electromagnetic wave. The total number of terms required in this expansion is $\sim 2\pi a/\lambda$, with a minimum of one. Thus for $2\pi a/\lambda \ll 1$ the first term, representing the dipole radiation, is sufficient. The number of terms required can be understood with the help of the 'localization principle' (van de Hulst, 1957; Bryant and Cox, 1966) which states that a term of order n in the multipole expansion of the scattered radiation corresponds to a ray passing the center of the sphere at a distance $n\lambda/2\pi$. (The basis for this principle is the same as in partial-wave analysis in quantum theory: the nth term is associated with an orbital angular momentum h/λ at an impact parameter $n\lambda/2\pi$.) Thus the series converges shortly after n exceeds $2\pi a/\lambda$, because higher terms correspond to rays which do not pass through the sphere.

If the contributions of the successive terms in the multipole expansion are added one at a time to form contour diagrams of the type in Fig. 7, only the dipole term (n=1) individually contributes a feature which is still readily apparent after the sum is taken over all terms. The quadrupole term moves the boundary between positive and negative polarization toward larger size parameters for small scattering angles; it also is primarily responsible for the positive feature at $x \sim 3$ and $\alpha \sim 110°$. The negative features for $2\pi a/\lambda \sim 4\text{-}8$ arise as the combined result of a few terms with $n \sim 2\pi a/\lambda$ and just smaller values of n. For larger size parameters the sharp feature in the polarization for $\alpha \sim 180°$, called the 'glory', also arises from the few terms with $n \sim 2\pi a/\lambda$. This feature can thus be associated with edge (grazing) rays which set up surface waves on the sphere (Kerker, 1969; van de Hulst, 1957; Bryant and Cox, 1966). The surface waves reradiate in all directions, but, because there are focal points in the directions $\alpha=0$ and 180°, the energy is concentrated in the forward and backward directions. For $\alpha=0°$ the effect is drowned in the

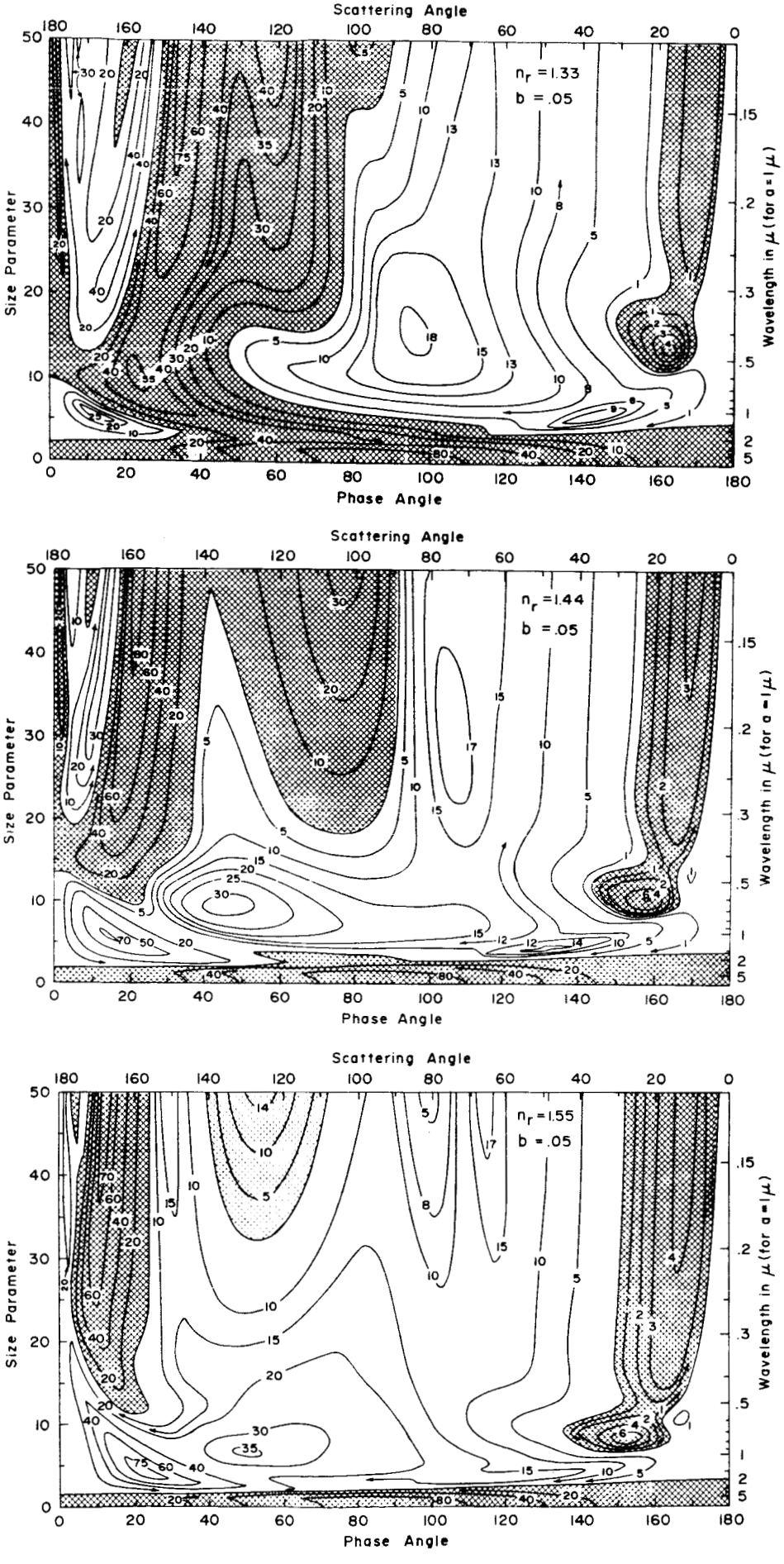

Fig. 8. Contour diagrams of the percent polarization for single scattering of unpolarized light by a size distribution of spheres.

The shaded areas indicate positive polarization ($I_r > I_\ell$) and the unshaded areas indicate negative values.

The size parameter is $2\pi a/\lambda$.

a is the effective mean radius and b=.05 the effective variance for the size distribution, for which the particular form was $n(r)=r^{(1-3b)/b}\, e^{-r/ab}$.

A comparison of the three diagrams illustrates the effect of the refractive index on the polarization.

much stronger diffracted light, but for $\alpha=180^{o}$ it is easily visible.

Effect of refractive index. The variation of the polarization with refractive index is illustrated in Fig. 8. The primary changes which occur in the different features can be understood on the basis of the physical origin of the features. The location of the rainbows moves in accordance with Snell's law and geometrical optics. The relative contribution from Fresnel reflection increases. The island due to anomalous diffraction moves to a smaller size parameter as n_r increases, because of the reduced ratio of the wavelength of rays inside the particle to the wavelength of the rays outside the particle.

In the case of spherical particles the variations of the polarization with refractive index can readily be used to establish the refractive index of the particles. An example of this for the clouds of Venus is given in Section 6.

Nonspherical particles. In the preceeding sections we mentioned differences and similarities in the scattering behavior of spherical and nonspherical particles which are predictable on theoretical grounds. Accurate numerical results for nonspherical particles have been obtained for only a few specific shapes. However, laboratory and field measurements are available in several different cases, and the prospects are good for obtaining improved laboratory data in the near future.

The effect of nonspherical shapes on scattered light depends on the size of the particles. For particles which are much smaller than the wavelength and made of isotropic material nonsphericity causes deviations from perfect Rayleigh scattering and these deviations are similar to those which occur for spherical anisotropic particles. However, for the wavelength range of potential interest for an MJS photopolarimeter the only deviations from isotropic Rayleigh scattering of relevance are those due to anisotropic gas molecules; and in this case the effect of the reduced polarization for anisotropic molecules is nearly cancelled by the increased cross-section of such particles. The radiation scattered from any size or shape of particle arises from oscillations of the electrons in the particle excited by the incident wave. Thus the radiation described as that from a series of multipoles can be imagined to have its origin in the density distribution of oscillating dipoles. It is therefore clear that for particle sizes comparable to the wavelength differences in the scattering for spheres and nonspheres will occur. These differences are difficult to predict for particles with $r\sim\lambda$ other than through accurate computations. However, for $x\gtrsim 5$ the effects due to surface waves must be modified for nonspherical particles, and in particular the features arising from the focusing of energy in the backscattered direction should tend to disappear as the particle shape deviates increasingly from spherical. For particles much larger than the wavelength major differences between the results for spherical and nonspherical particles exist. The absence of a glory for cylindrical particles has been demonstrated with exact computations (Liou, 1972 a,b). As we indicated above other features also depend specifically on the spherical shape, e.g, the rainbows and the island in the polarization due to anomalous diffraction. This is verified by laboratory and field observations (Section 5) and theoretical work.

Infinitely long circular cylinders are the nonspherical particles which have been studied numerically in greatest detail (e.g., Kerker, 1969; Liou, 1972 a,b). For light incident perpendicular to the axis of such cylinders the cross-section of the particles is circular and in the limit of geometrical optics the polarization is the same as for spheres. For oblique incidence the rainbows are distorted in position and magnitude. The glory is absent for any particle orientation. Circular cylinders do not represent a particle form which is likely to be encountered very often in planetary atmospheres, but the calculations for such particles do help to provide an understanding of variations in the scattering which occur with changes in the particle shape.

Calculations have also been made for infinitely long hexagonal cylinders in the limit of geometrical optics (e.g., Jacobowitz, 1971). These are relevant to the needle crystals which often predominate in cirrus clouds. The computations for this case illustrate the absence of rainbows for particles which do not have a circular cross-section. However, for hexagonal ice crystals a new feature appears in the scattered light: at $\lambda\sim 22^{o}$ there is a concentration of light due to the $\ell = 2$ (twice refracted) rays. This 'halo', like the rainbow for spheres, occurs at an angle of minimum deviation. Its location depends on the prism angle (in this case 60^{o}) and on the refractive index. Features of this type can be useful for particle identification in situations in which there are a small number of suspected compositions for which the refractive index and crystal habit can be obtained in the laboratory.

Theoretical computations have also been made for particles of a number of other shapes (including spheroids (Greenberg, et al., 1961), elliptical cylinders (Yeh, 1964) and several different shapes of totally reflecting particles. Furthermore, numerical methods are available (e.g., Kerker,1969) which can be applied to particles of almost any shape, and with modern computers these may prove to be useful.

Laboratory measurements have provided a powerful means for studying the scattering properties of nonspherical particles. Lyot (1929), using a visual polarimeter, was the first to obtain accurate measurements of the polarization properties as a function of scattering angle. More recently Pritchard and Elliot (1960) and Holland and Gagne(1970) have used photometric methods to measure all of the significant phase matrix elements for a few different types of particles. Greenberg, et al.(1961) have employed microwave analog techniques, with both the particle size and wavelength in the microwave region, to investigate the effects of nonspherical particles. However, it has recently been demonstrated that lasers can be used to accurately measure the phase matrix for single scattering by spherical and nonspherical particles (Blau, et al.,1970), and it is likely that this technique will be widely used in the future for investigating nonspherical particles.

Since there are so many different possible nonspherical particles it is reasonable to ask what we can be confident of learning from measurements of scattered light for cases in which the particles may be of any shape. If observations are made over a wide range of scattering angles it will certainly be possible to distinguish spherical particles from nonspherical ones. This is in itself a significant conclusion which is indicative of the phase (liquid or solid) of the particles. Of course if the particles are spherical more details on their microstructure can be extracted, and some possibilities for additional information exist for nonspherical particles of a regular shape. If the particles are irregular in shape it will still be possible to determine whether the particle size is comparable to or much larger than the wavelength from the dependence or independence of the cloud particle polarization on wavelength.*

Regardless of the particle shape the polarization can be used to separate the scattering by gas molecules from that due to cloud particles. The simple form of the polarization for Rayleigh scattering as a function of scattering angle allows it to be distinguished from the cloud scattering. The strong wavelength dependence of the cross-section (or optical thickness) for Rayleigh scattering ($\propto \lambda^{-4}$), together with the broad wavelength interval of the photopolarimeter proposed for MJS, would allow the measurement of the number of particles in a vertical column above the cloud for a range corresponding to cloudtop pressures of ~10mb to ~1atm. The derived gas amount refers to only gas above the clouds if the mean-free-path in the cloudtops is sufficiently small, as is the case for terrestrial clouds. In the case of a diffuse haze the derived amount refers also to gas mixed with the haze in the region where the first few scatterings occur (Section 4), and thus the derived pressure level does not refer to a sharp top of the particulate region of the atmosphere. This does not represent a problem, however, and indeed the distinction between a diffuse haze, dense cloud or some intermediate case is a valuable one which can be obtained from the polarization. The possibility of doing this can be easily understood because as the zenith angle of observation increases from 0^{o} (i.e., normal to the planet's surface) toward 90^{o} the contribution to the polarization from Rayleigh scattering increases dramatically in the case of gas above a cloud deck, while the relative contribution of gas and particulates remains essentially constant in the case of a diffuse haze.

---

*Wavelength dependence of the polarization due to variations of the refractive index (n_r) or the particulate absorption (n_i) must also be considered. However in most cases these will be either small or easily accounted for. The great majority of materials have a normal dispersion for n_r in the wavelength range of interest, and moreover the effects of a smoothly varying n_r can often be detected. Variations of n_i can cause large changes in the albedo, but the major effect in on the total intensity, I, not the intensity of polarized light, I_p; thus the degree of polarization, I_p/I, is affected in a simple way. Changes in the albedo can therefore be accounted for if photometric measurements are included.

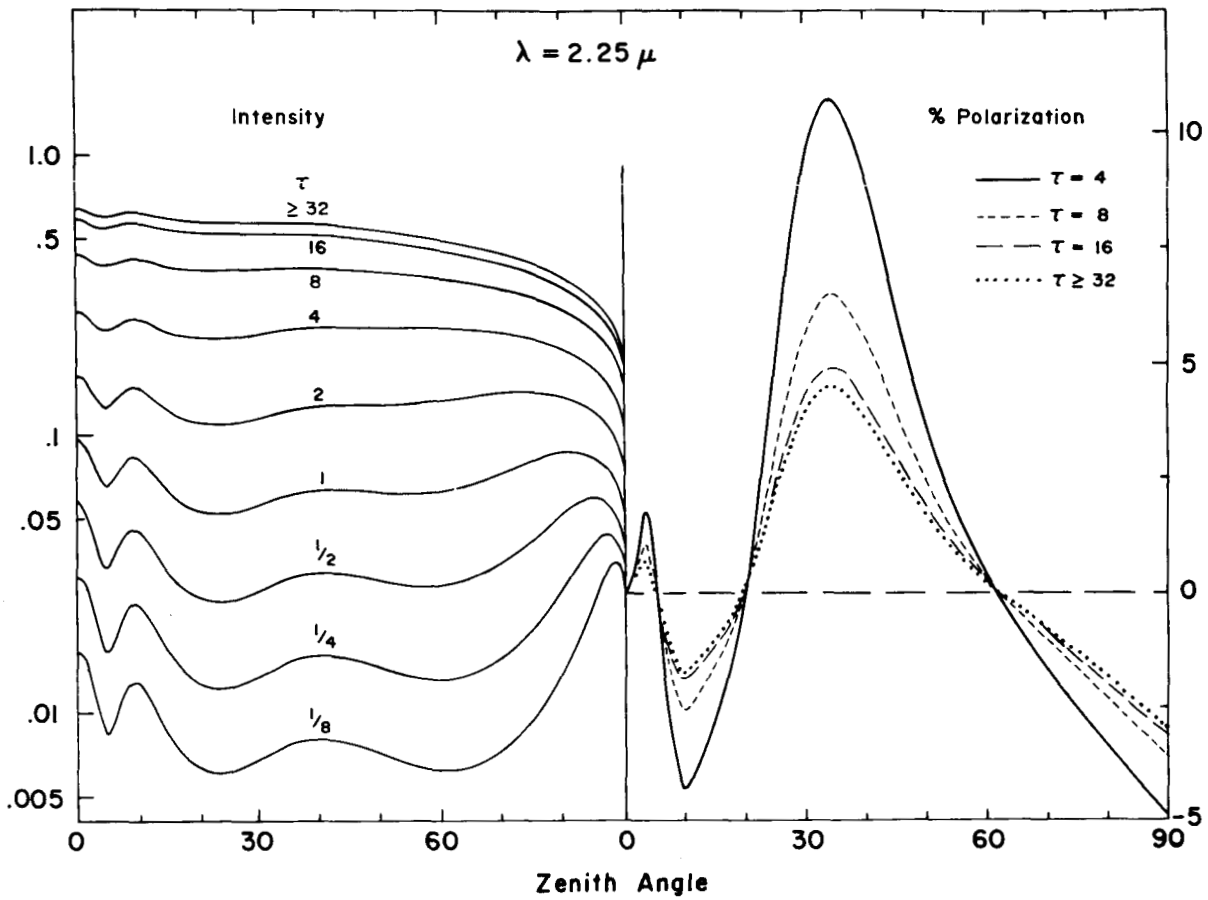

Fig. 9. Intensity and percent polarization (-100 Q/I) of sunlight reflected by a plane-parallel water cloud with the sun overhead ($\theta_o = 0^o$). The wavelength is 2.25μ and results are shown for several optical thicknesses, τ. On the horizontal axis is the zenith angle of the reflected light, $\theta = \cos^{-1}\mu$. The calculations are for the size distribution (9) with a = 6μ and b = 1/9.

4. MULTIPLE SCATTERING

It has been demonstrated that single scattered radiation carries a detailed signature of the scatterers. Thus a large amount of information on atmospheres, surfaces and interplanetary particles can potentially be obtained from measurements of scattered radiation. Indeed, even for in situ atmospheric measurements of cloud and haze particles it is difficult to find more reliable means for analyzing the nature of the particles than through measurements of single scattered light (as is done with a nephelometer).

However, in most of the cases of relevance to an MJS mission the radiation has been multiply scattered and the observable signal represents an average of photons scattered different numbers of times at all potential scattering angles. This process tends to smooth out features which occur in the radiation as a function of scattering angle at a given wavelength. Spectral absorption features usually become stronger with multiple scattering, but these features then represent some average over the entire depth to which the photons have traveled. In either case to interpret the observations it is necessary to be able to model the multiple scattering process. Multiple scattering computations are also necessary before observations are made in order to find the radiation characteristics which best survive the multiple scattering.

There are a number of different ways of computing the multiple scattering of light, some including the effects of polarization. Several of these methods have been briefly discussed by Hansen (1971b,c). Most of these are restricted to the case of a locally plane-parallel atmosphere, but in practice this special case is almost always sufficient. The computations in this section were made with the so-called 'doubling method' (van de Hulst and Grossman, 1968; Hansen, 1971b); the same approach is valid for vertically inhomogeneous atmospheres in which case it is usually called the 'adding method'.

Fig. 9 shows the computed intensity and polarization at λ = 2.25μ for the reflection of sunlight from a plane-parallel water cloud for different optical

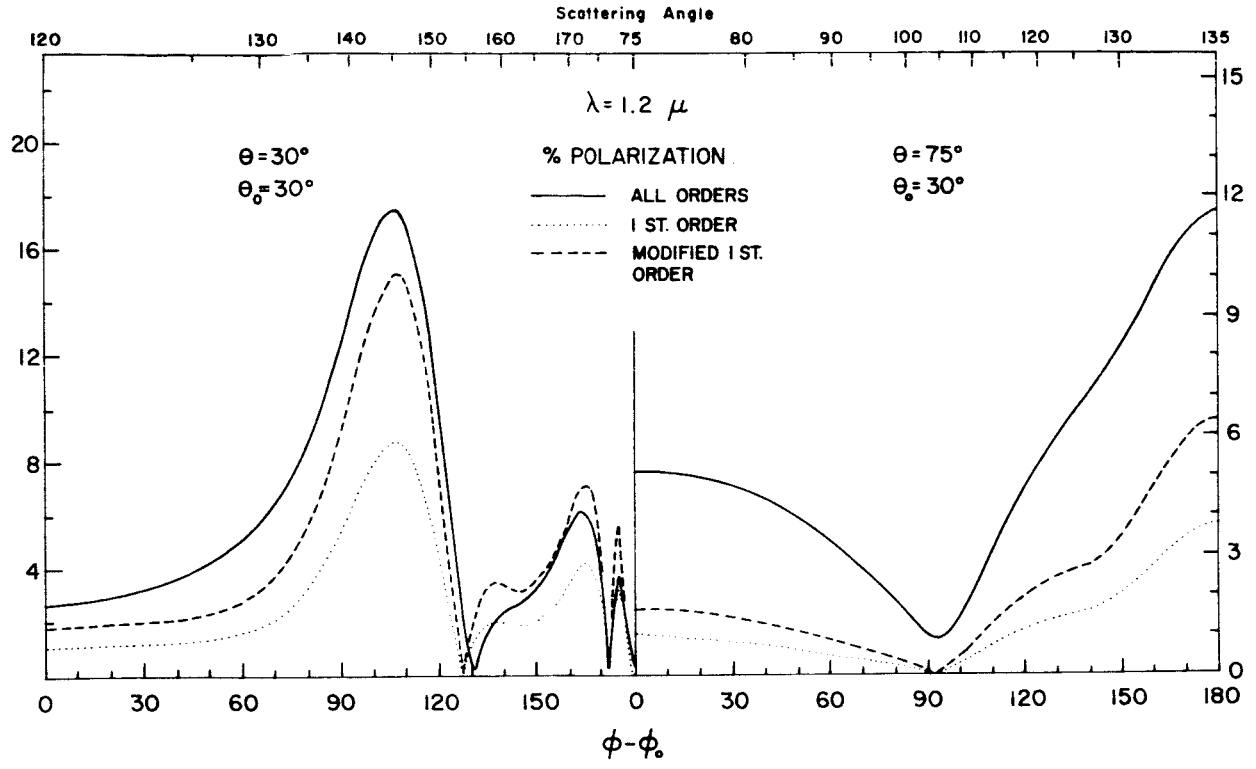

Fig. 10. Percent polarization as a function of azimuth angle, $\phi-\phi_o$, of sunlight reflected by a plane-parallel water cloud for $\lambda = 1.2\mu$, $\tau = 4$ and the indicated values of θ and θ_o. The curves for all orders are 100 $(Q^2 + U^2 + V^2)^{\frac{1}{2}}/I$, those for first order are computed including only the contribution of single scattering in the numerator, $(Q^2 + U^2 + V^2)^{\frac{1}{2}}$, and those for the modified first order are explained in the text. The calculations are for the size distribution (9) with $a = 6\mu$ and $b = 1/9$.

thicknesses. The particle size distribution is given by (9) with $a = 6\mu$ and $b = 1/9$ which is representative for terrestrial fair weather cumulus clouds. For this case the single scattering albedo is ~ 0.99 so there is a great amount of multiple scattering. The single scattering features in the angular distribution of the intensity are practically lost due to the multiple scattering. A 'limb darkening' for $\theta \to 90^o$ is introduced by the multiple scattering; this feature depends on the optical thickness, the single scattering albedo and the asymmetry of the phase function, but it is not sufficiently sensitive to the nature of the scatterers to be very useful for particle identification. The primary effect of multiple scattering on the degree of polarization is to reduce its value without changing its general form, as was realized by Lyot (1929) and Coffeen (1969).

The format of Fig. 9 is appropriate for comparison to observations, and thus for a practical test of how well single scattering features in the angular distribution of the reflected light survive the smoothing effect of multiple scattering. The intensity is plotted on a logarithmic scale which is consistent both with the presentation of most observers and with the observational accuracies which have been obtained. The polarization is plotted on a linear scale which allows differences of a few tenths of a percent polarization to be resolved, because accuracies of this order are obtained in observations (Lyot, 1929; Coffeen and Gehrels, 1969).

Fig. 10 shows the degree of polarization (say I_p/I where I is the total intensity and I_p is the intensity of polarized light) computed for water clouds at $\lambda=1.2\mu$ and a comparison to an approximation for the polarization, I_p'/I, in which only the contribution of single (first order) scattering is included in the numerator. Also illustrated is a modified approximation which is based on the assumption that diffracted photons may be counted as being unscattered; i.e., photons are allowed to contribute to I_p' according to the single scattering phase matrix on their first nondiffraction scattering (Hansen, 1971c). This figure illustrates that the single scattering is primarily responsible for the polarization.

The general effect of multiple scattering on the intensity and polarization can be readily understood. Photons emerging from the atmosphere after several scatterings

are practically unpolarized and they have an intensity which is more or less isotropic. Thus in the degree of polarization, I_p/I, only the photons scattered once or a small number of times contribute significantly to I_p. The shape of the polarization vs. scattering angle is therefore determined by the scatterers in the top of the atmosphere, where the optical thickness is $\lesssim 1$. If variations of the properties of the scatterers occur at greater depths the only significant effect on the degree of polarization is through the total intensity; this is of little concern if the intensity is measured.

The region of the atmosphere where $\tau \lesssim 1$ is that of the greatest interest: this is approximately the depth to which we can see visually and, unless the particles are smaller than the wavelength, it is also radiatively effective in the thermal part of the spectrum.

5. APPLICATION TO EARTH CLOUDS

Polarization observations of the Earth's atmosphere have not played a major role in atmospheric studies. There are several reasons for this in addition to the fact that the particles and gas in our atmosphere can be sampled in situ. Until recently it has not been possible to make theoretical computations for phase matrices which could be expected to represent the real atmosphere. Furthermore, in the case of clouds useful observations from the ground are not possible because transmitted sunlight is practically unpolarized. However, recently at least one series of aircraft measurements of cloud polarization (described below) has been made, and satellite observations by the Soviet Union have been reported (Vinnichenko, 1972), though the details are not yet available. Satellite observations of the polarization of reflected sunlight have been recommended for measuring cloud optical properties (COSPAR, 1972) as well as for monitoring terrestrial aerosols (NASA, 1971).

Potential cloud information. A discussion of potential information in polarization observations of terrestrial clouds has been given by Hansen and Coffeen (1972). The primary information appears to be the following:

1) particle phase. It is not practical to compute the polarization for realistic models of ice clouds because the particles are anisotropic and of various shapes, but it is certain that the polarization for ice clouds is drastically different from that for water clouds. For example, the rainbow and glory do not exist for ice crystals. Thus it would be possible to make measurements across the rainbow region to identify water clouds. However, there are also characteristic differences between ice and water at other scattering angles, and it will be necessary to make systematic observations on ice clouds before it can be determined what measurements most conveniently yield the particle phase.

2) particle size. This can be obtained for water clouds from comparisons of theoretical computations to observations. A number of different features could be used, but the theoretical figures presented below suggest that measurements at scattering angles ~100 degrees would provide a simple means for particle sizing.

3) cloud height. The cloud height can be obtained from the polarization of reflected sunlight by means of measurements in the visual and ultraviolet. The amount of Rayleigh scattering at these wavelengths can be converted to the cloud-top pressure. The potential accuracy with which it should be possible to obtain the cloud height using this method is ~1 km.

4) water content. If the cloud optical thickness is known it can, together with the particle size, be converted to the liquid water content in a vertical column. For water clouds the optical thickness can be obtained from the polarization, as indicated by Fig. 9. (The polarization is more sensitive to the optical thickness at shorter wavelengths where the absorption is negligible.) The derivation of the liquid water content will require either the assumption that the particle size is approximately constant with height in the cloud or that a systematic variation with height can be allowed for based on the cloud type.

Theoretical Computations in the Infrared. Coffeen and Hansen (1972) have begun a theoretical and observational program to explore the information which can be obtained from polarization observations of terrestrial clouds. The first observations were restricted to the near-infrared region ($1\mu \lesssim \lambda \lesssim 3.5\mu$) which is sensitive to the particle size but which can

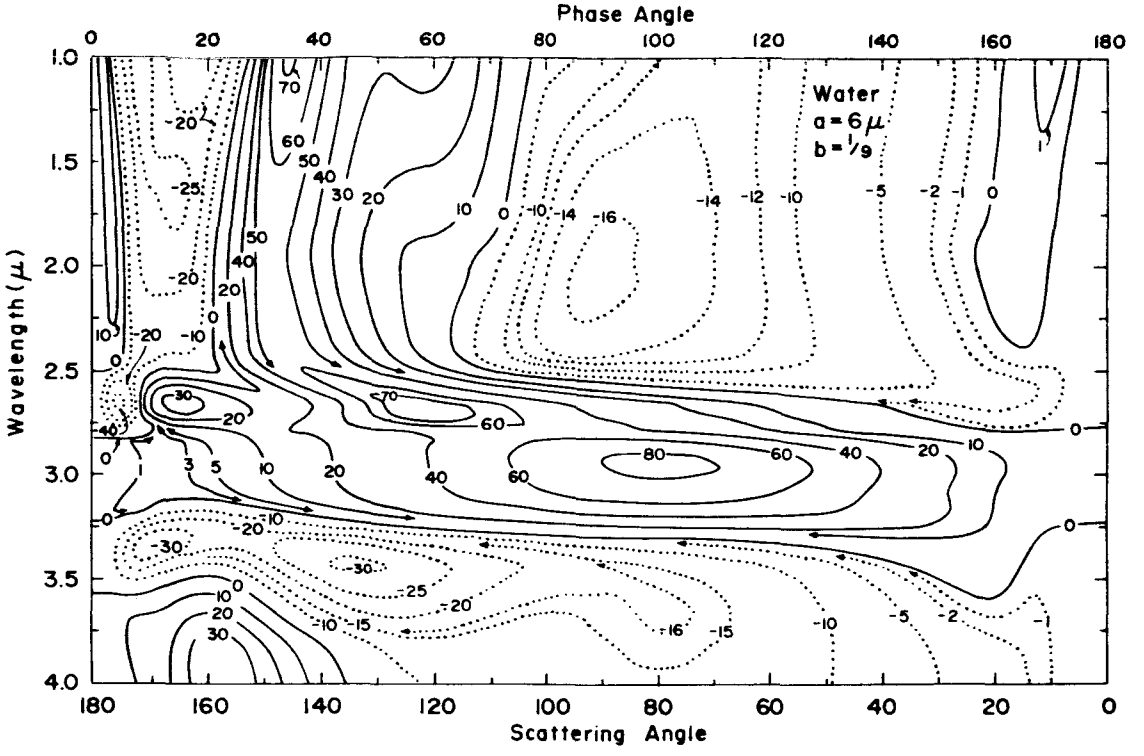

Fig. 11. Contour diagram of percent polarization as a function of scattering angle and wavelength for single scattering by a size distribution of water particles. The size distribution is that given by (9) with a = 6μ and b = 1/9. Solid curves are used for positive polarization and dotted curves for negative polarization.

not be used for measuring cloud heights. In this subsection we will illustrate some theoretical curves for single scattering by water clouds in the near infrared. These computations are useful for determining the optimum wavelengths and directions for observations.

Fig. 11 shows the percent polarization as a function of scattering angle and wavelength in the near-infrared for single scattering by water particles which follow the size distribution (9) with a ≈ 6μ and b = 1/9. The strong positive polarization running horizontally across the diagram for wavelengths near 3μ is due to Fresnel reflection from the outside of the particle. In this wavelength region water is strongly absorbing so there is practically no penetration of the particles by light rays. For wavelengths less than 2.5μ the narrow positive feature at scattering angles near 180 degrees is the glory. The large positive polarization with its maximum near the scattering angle 145 degrees is the primary rainbow, while the second rainbow is just apparent near 120 degree scattering angle. For scattering angles between 20 and 100 degrees and wavelengths $\lesssim$ 2.5μ most of the light is from rays refracted through the particles with no internal reflections; this is negatively polarized. The region between the glory and the rainbow is also negatively polarized; because of interference features the polarization in this region is sensitive to the shape of the size distribution. For wavelengths between 3.25 and 4μ the wavelength is close enough to the mean effective size that the concepts of geometrical optics have little applicability. This is the transition region between Rayleigh scattering and large particle scattering, and hence the polarization is strongly dependent on the mean effective radius, a.

Figs. 12 and 13 show the percent polarization for two additional size distributions of water particles, with the values for the mean effective radius being 10μ and 20μ, respectively. For the range of b typical of terrestrial water clouds (~ .10-.25) the polarization in the near-infrared is much less sensitive to b than it is to a.

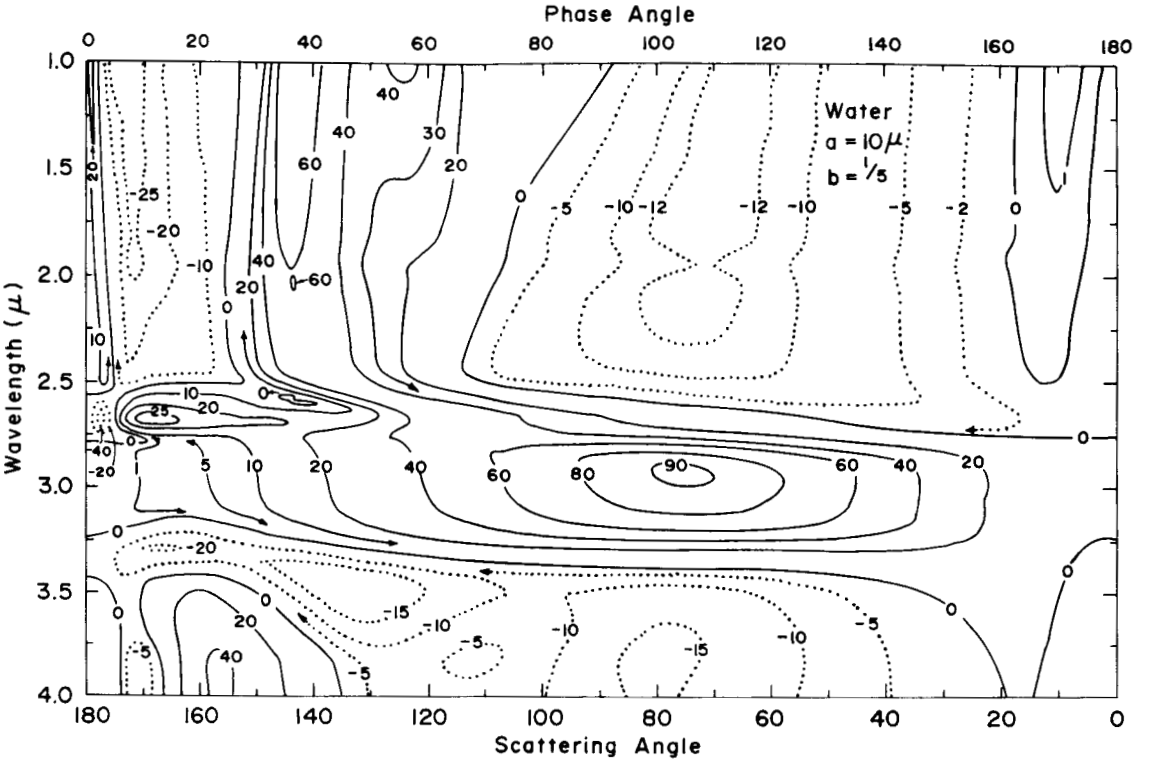

Fig. 12. Same as Fig. 11, but here a = 10μ and b = 1/5.

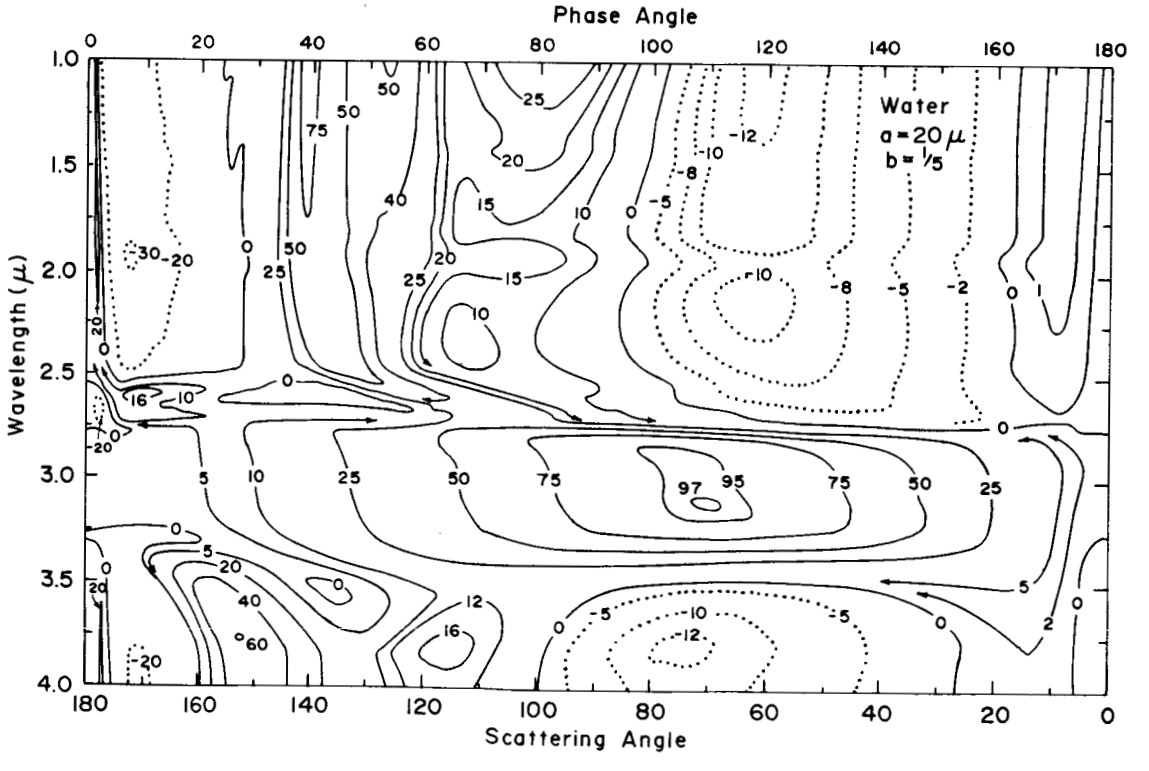

Fig. 13. Same as Fig. 11, but here a = 20μ and b = 1/5.

A comparison of Figs. 11-13 illustrates the effect of the particle size on the polarization in the near-infrared. At the longest wavelengths, $\lambda \geq 3.5\mu$, the polarization changes drastically between the different figures, the glory, rainbow and other features of geometrical optics becoming more distinct with increasing particle size. The positive polarization at $\lambda \sim 3\mu$, due to Fresnel reflection, does not change much with increasing particle size, because it is already near the limit of geometrical optics for $a = 6\mu$. The primary rainbow becomes narrower with a somewhat larger peak value as the particle size increases. The curvature in the contours near 1.95 and 1.45μ is introduced by the absorption bands of liquid water at those wavelengths; this absorption of course preferentially attenuates the rays with longer pathlengths inside the particles.

For wavelengths less than 2.5μ and scattering angles ~100 degrees the polarization increases with particle size. This is due to the increasing predominance of Fresnel reflection at those angles, as we will explain here. The features described above in terms of geometrical optics cannot be precisely localized to the scattering angle regions which they would occupy in the limit of infinitely large a/λ. This particularly affects transparent particles in the region where Fresnel reflection would dominate in the geometrical optics limit because the intensity of these externally reflected rays is small. Thus the spreading of even a small fraction of the negatively polarized twice-refracted rays into the region of scattering angles ~100 degrees can easily swamp the positive polarization. Conversely, as the wavelength decreases or as a increases the negative polarization tends to be better confined to the region it occupies in the limit of geometrical optics, and hence a positive maximum appears in the polarization at scattering angles ~100 degrees (cf. Fig. 13 for $\lambda \sim 1\mu$). The variation of the polarization for scattering angles ~60-100° provides a straightforward method for particle sizing, as illustrated below.

Cloud Observations. Measurements of the polarization of sunlight reflected by terrestrial clouds were made by Coffeen and Hansen (1972) on a series of flights on the NASA Convair 990. The polarimeter was mounted in a side window of the aircraft and could scan in a single vertical plane parallel to the main axis of the plane. Observations were made at λ = 1.25, 1.6 and 2.25μ. The results are presently being analyzed, but some of the measurements which have been reduced are illustrated here.

Fig. 14 shows polarizations measured over two different cloud systems on different days. These two clouds were special in the sense that they were the only ones for which a rainbow could be seen from the airplane with the naked eye. These cloud systems were relatively uniform and thus the polarization curves are quite smooth. A comparison of these curves with the theoretical computations indicates that the mean effective particle radius in the tops of these clouds was $20\text{-}25\mu$.

Rainbows were detected in the polarization for all clouds which were observed at the appropriate scattering angles and known (from their altitude and visual appearance) to be of the water type.

The most convenient indicator of particle size is the crossover point (neutral point) from positive to negative polarization at $\lambda=2.25\mu$. The phase angle of this neutral point increases monotonically as the average particle size increases, and at $\lambda=2.25\mu$ it has a wide potential range. The dependence of the neutral point on particle size is sufficiently simple that even a rather dull computer can be trained to use it automatically, and hence it should be useful for satellite observations.

Fig. 15 shows observations of a thick cirrus cloud system. These two sets of observations were taken on the same day and they were the only cirrus observations in the data which have been reduced so far. Therefore conclusions should be reserved, but it is clear that the polarization for ice clouds is greatly different from that for water clouds, and in ways which can be understood. There is no rainbow for cirrus clouds. The broad positive polarization feature must be due to Fresnel reflection from the outside of the particles; this is expected since cirrus crystals are known to be large. The observations did not reach the region of the "22° halo" (which, for the refractive index of ice at this wavelength, would occur at the phase angle ~161°).

Fig. 16 shows a series of observations over water clouds which were taken consecutively on one flight. The first observations, on the left, were over a front

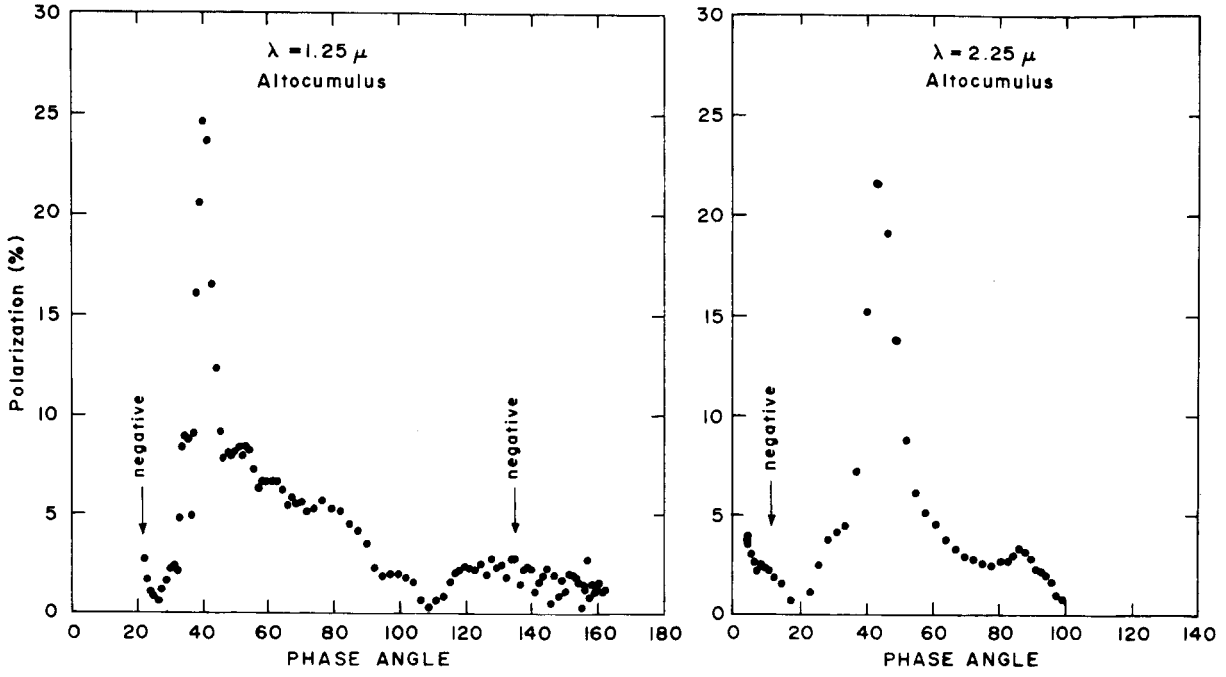

Fig. 14. Percent polarization of reflected sunlight observed at λ=1.25μ (left) and λ=2.25μ (right) over two different clouds. "Negative" is used to indicate branches of the curves where the direction of polarization is predominately parallel to the plane of scattering.

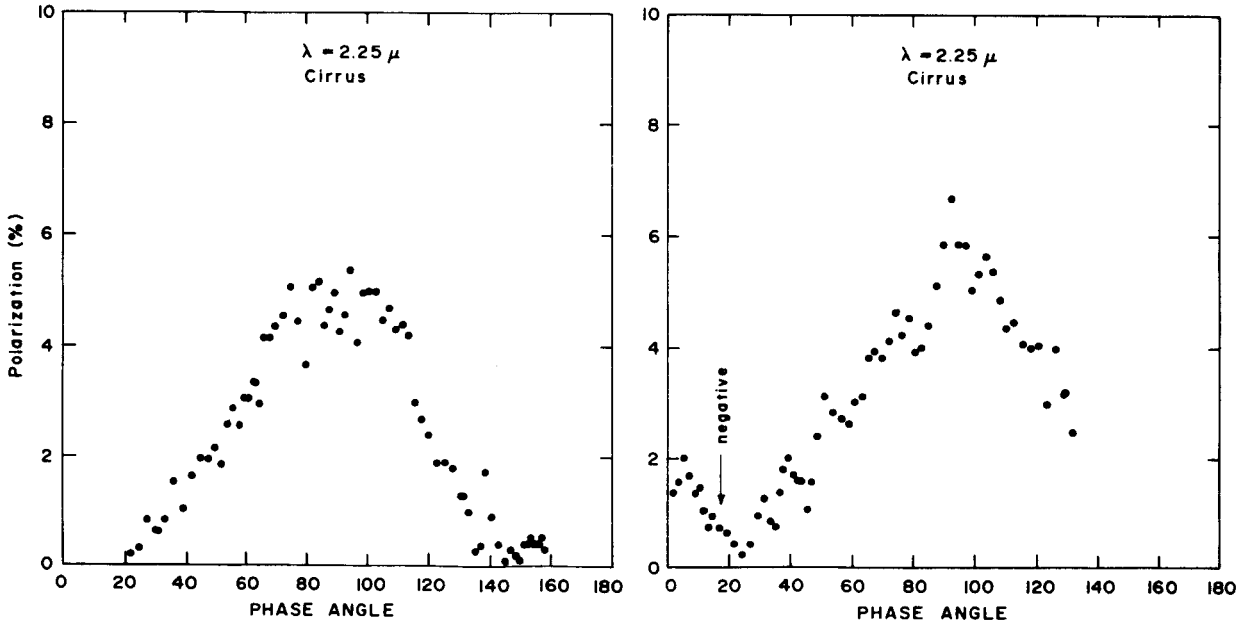

Fig. 15. Percent polarization of reflected sunlight observed at λ=2.25μ over cirrus clouds. The two sets of observations were taken on the same day over clouds separated by several miles.

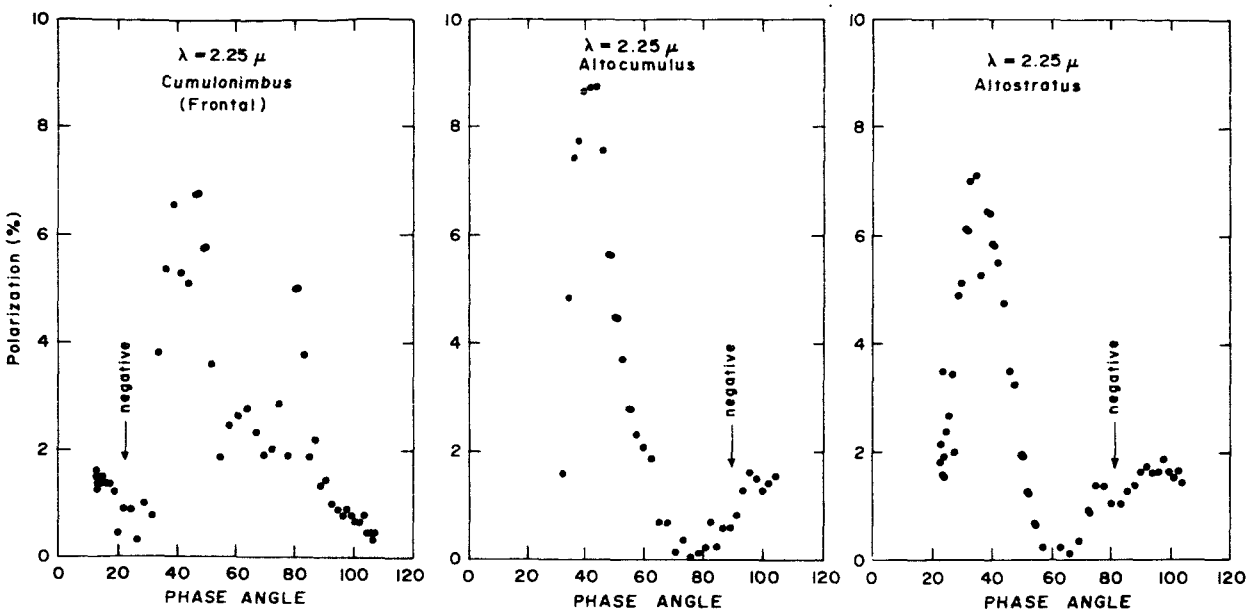

Fig. 16. Percent polarization of reflected sunlight observed at λ=2.25μ over three different clouds which were encountered consecutively in time from left to right. The observations on the left were over a narrow front of raining clouds. The other two sets of observations were taken behind the front and for the latter cases the cloud types indicated above are uncertain, except for the fact that they were fair weather clouds.

of raining cumulus clouds at least several kilometers long and a fraction of a kilometer wide. The clouds were very turbulent and nonuniform in brightness, thus accounting for the appearance of the polarization curve. The apparent neutral point for the polarization indicates an effective particle radius of at least 30μ. The clouds immediately behind the front (center part of Fig. 16) had much smaller particles, about 10μ in radius. Still further away (right part of Fig. 16) were clouds with a mean size of about 5μ.

Although the observational programs for terrestrial clouds are at an early stage, the results tend to confirm theoretical expectations and they are indicative of the high information content in the polarization.

6. APPLICATION TO VENUS

The polarization of sunlight reflected by Venus was first measured by Lyot in 1922 (Lyot, 1929). The amount of polarization observed was small (Fig. 17), but, because of the high accuracy of the measurements and the sensitivity of the polarization to the optical properties of the scattering medium, the observations contain a large amount of information. Coffeen and Gehrels (1969) extended the measurements to several wavelengths from the near-ultraviolet region (λ = 0.34μ) to the near-infrared region (λ = 0.99μ).

The fact that the mass of the Venus atmosphere is large (surface pressure ~ 100 atm) assures that the polarization observations refer primarily to photons multiply scattered within the atmosphere and not to reflections from a solid planetary surface. A complete theoretical interpretation of the observations must, therefore, be based on solutions of the radiative transfer equation. Exact solutions for a Rayleigh atmosphere (gaseous molecules or particles with radius $r \ll \lambda$) have long been available, but, as shown in Fig. 17, Rayleigh scattering produces a polarization at visible wavelengths that is much larger than the polarization observed on Venus.

It thus follows that in the atmosphere of Venus there must be cloud or haze particles which are primarily responsible for the polarization. Indeed, laboratory measurements, as well as theoretical calculations for single scattering by spherical particles, indicate that the polarization of Venus is characteristic of scattering by particles with $r \sim \lambda$. Using his laboratory measurements, Lyot

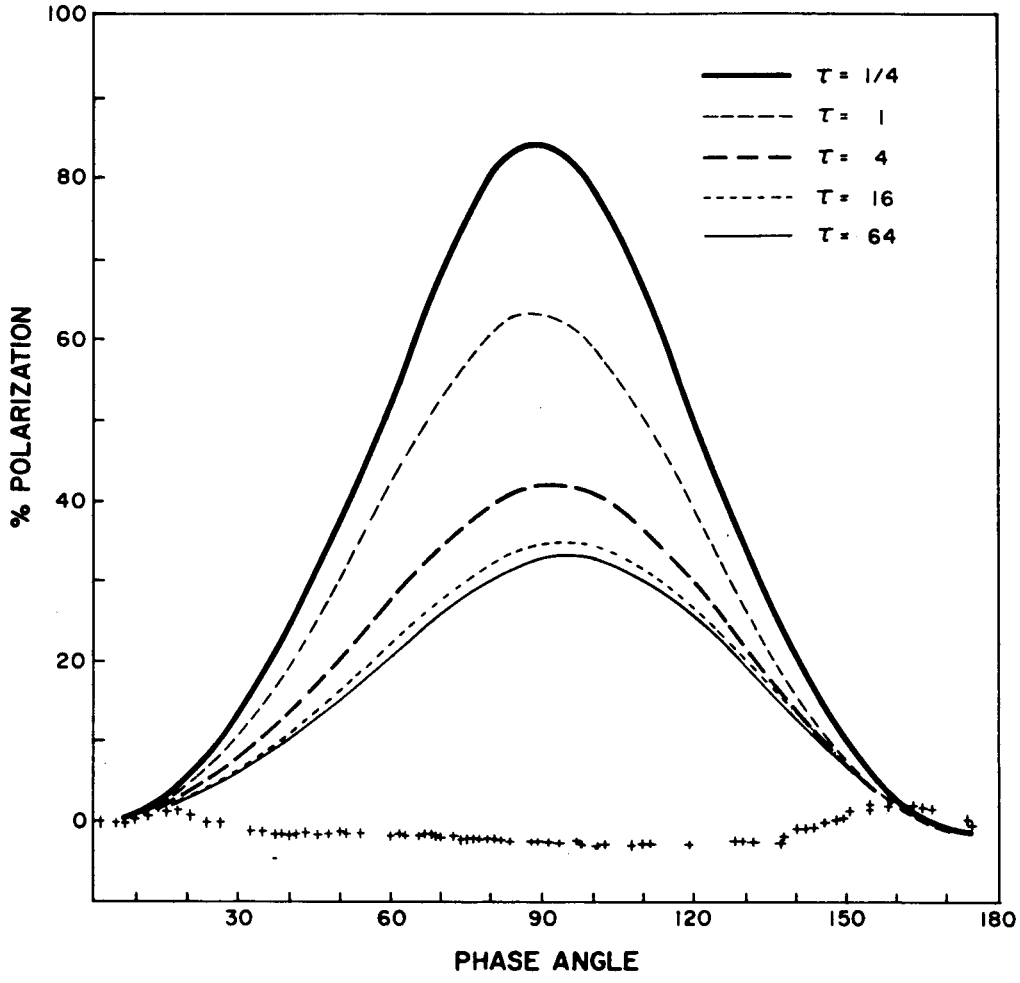

Fig. 17. The pluses represent Lyot's measurements of the polarization of the visual light reflected by Venus. The theoretical curves are for Rayleigh atmospheres of different thicknesses.

(1929) found that clouds composed of water drops (refractive index $n_r \sim 1.33$) with $r \sim 1.25\mu$ were in reasonably good qualitative agreement with his observations of Venus. Coffeen (1969),on the other hand,compared the observations of Coffeen and Gehrels (1969)with calculations for single scattering by spheres and concluded that $1.43 \leq n_r \leq 1.55$ and $r \sim 1.25\mu$.

Hansen and Arking (1971) obtained numerical solutions for the multiple scattering of light (including polarization) from a plane parallel atmosphere consisting of a mixture of spherical particles and Rayleigh scatterers. The results were integrated over the visible part of the planetary disk to allow a comparison with the observations of Venus. The polarizations obtained were found to depend upon the real refractive index* and the particle size distribution.

The effect of the size distribution can be accurately described by two parameters, the mean effective radius and the effective variance, as illustrated in Section 3. The calculations for the

*The imaginary part of the refractive index must be very small for the particles in the upper cloud layer on Venus, and the single scattering albedo must be close to unity. To account for the spherical albedo of Venus, which is less than 100%, it is possible to choose either a finite atmosphere with a partially absorbing ground or a single scattering albedo less than unity.Both of these alternatives were tested and within the thickness of the curves in Figs. 17-20, the results were identical; in view of the effect of multiple scattering discussed in Section 4 this is readily understandable.

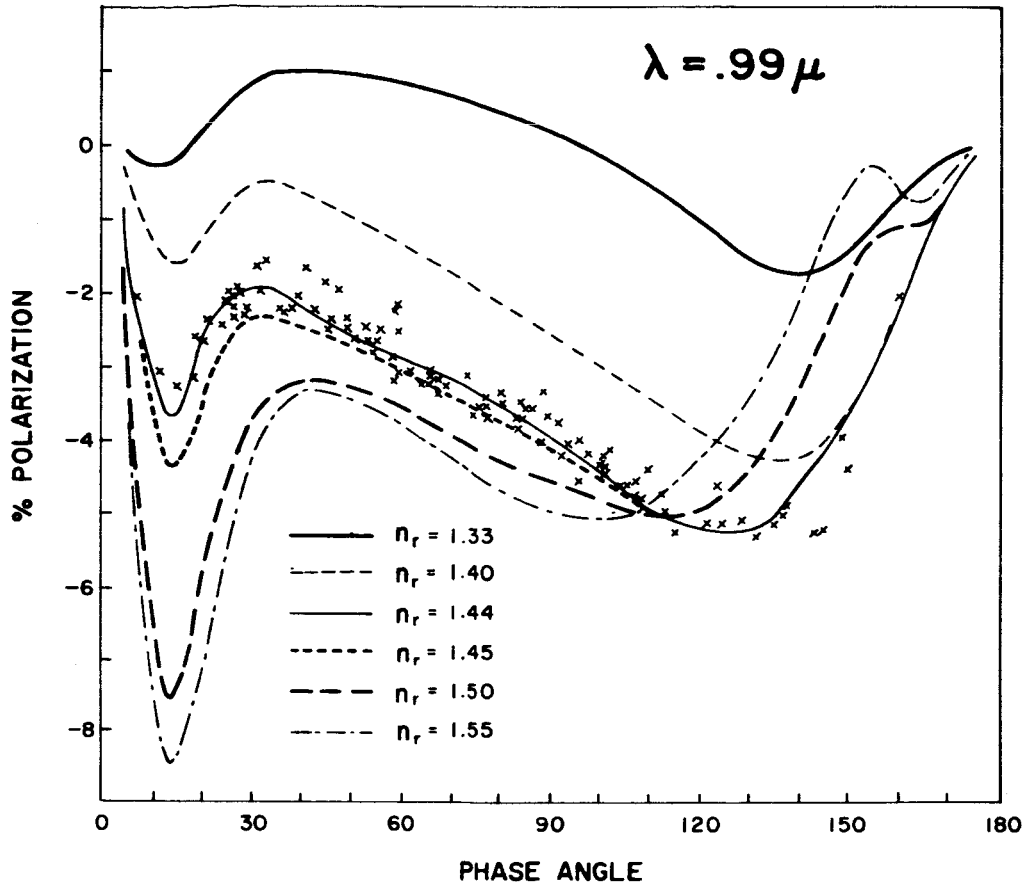

Fig. 18. The crosses show the observations of Coffeen and Gehrels of the polarization of Venus at a wavelength of 0.99μ. For each refractive index n_r the theoretical calculations are for the particle size giving best agreement with the observations for all wavelengths: $\bar{r}$ (λ=.55μ) = 0.7, 0.8, 1.1, 1.1, 1.2 and 1.2μ, respectively, beginning with n_r = 1.33. The curves for n_r = 1.44 and 1.45 are indistinguishable for phase angles greater than 110°. The albedo of Venus is assumed to be 90 percent at λ=0.99μ.

figures in this section were made for the size distribution (9) with the effective variance b = 1/9~.11, which yields good agreement with the observations. (As discussed below a closer fit to the observations can be obtained with b = .08.) Hence the results illustrated in Figs.18-20, showing polarizations as a function of the planet's phase angle,depend upon two parameters:the index of refraction, n_r, and the mean effective particle radius,$\langle r \rangle_{eff}$ = a. Alternatively the results depend on n_r and $\bar{r}$, the mean scattering radius (Hansen and Pollack,1970;Hansen, 1971c), where $\bar{r}$ and a differ by a few percent.* For observations at short wavelengths, where Rayleigh scattering is important because of its $1/\lambda^4$ dependence, the fractional contribution of Rayleigh scattering is an additional parameter.

The sensitivity of the theoretical computations to changes in the refractive index is illustrated by Fig. 18 which includes Coffeen and Gehrels' observations at λ = 0.99μ. For each refractive index that particle size is shown that gives the best overall agreement for all wavelengths from 0.34 to 0.99μ. The minimum near a phase angle of 15° is the glory, which arises from surface waves generated on sperical particles by edge rays;the glory is very broad at this wavelength because of the small size parameter x = $2\pi r/\lambda$. The broad maximum near a phase angle of 30° is the primary rainbow,which arises from rays internally reflected once in spherical particles; this feature becomes increasingly distinct toward shorter wavelengths.

*Hansen and Arking employed $\bar{r}$ instead of a; $\bar{r}$ varies with wavelength by a few percent for .34μ ≤ λ ≤ .99μ.Kattawar, et al (1971) incorrectly suggested that Hansen and Arking allowed the size distribution to vary with wavelength.

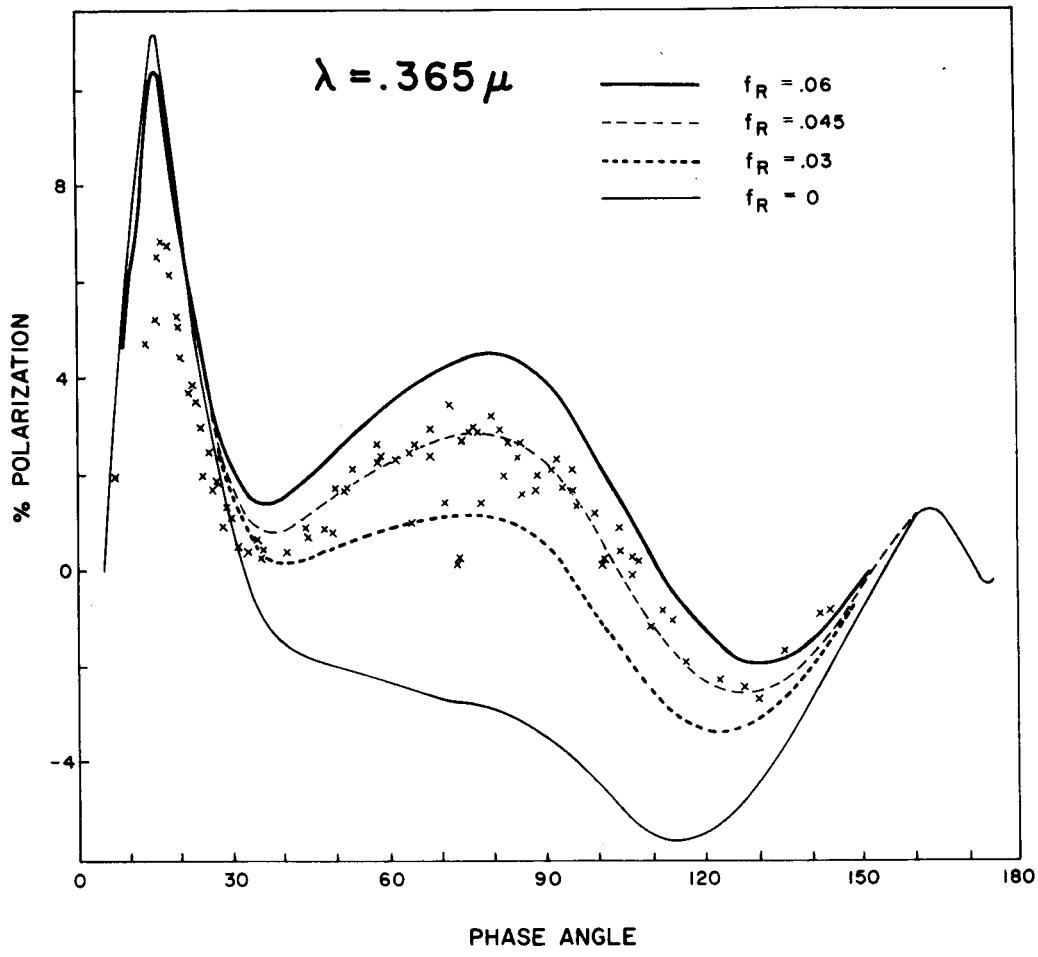

Fig. 19. The crosses show the observations of Coffeen and Gehrels at $\lambda = 0.365\mu$. The theoretical curves are computed with a fraction f_R of the phase matrix being Rayleigh scattering and a fraction $(1-f_R)$ being the Mie phase matrix for $n_r = 1.46$ and $\bar{r}(\lambda=.55\mu) = 1.1\mu$. The albedo of the planet is assumed to be 55 percent.

At visual and shorter wavelengths there is a nonnegligible contribution from Rayleigh scattering, which may be estimated best from the ultraviolet observations. Figure 19 shows the results of calculations at $\lambda = 0.365\mu$ for a model with a uniform mixture of spherical cloud particles and Rayleigh scatterers. The derived amount of Rayleigh scattering may then be used to obtain the pressure at a level of significant optical depth ($\tau \sim 1$) in the clouds; the result is ~50mb, which, for comparison, corresponds to the pressure in the earth's stratosphere at ~20km.

The observed magnitude of the polarization in the rainbow at $\lambda = .365\mu$ (Fig. 19) does not agree quantitatively with the theoretical result. However, more recent observations (Dollfus and Coffeen, 1970) show a maximum polarization of ~10%, in perfect agreement with the theory. It is conceivable that the old observations were in error, but it seems more probable that the polarization of Venus is variable in the UV, as is also suggested by polarization observations at other phase angles and by the presence of variable cloud features in UV photographs. The interpretation of such a variability should probably be connected with the variable ultraviolet markings on the planet.

The visual observations of Lyot and the intermediate-bandwidth observations of Coffeen and Gehrels at $\lambda = 0.55\mu$ are shown in Fig. 20. The theoretical curves illustrate the sensitivity of the polarization to variations in the particle size, and they indicate that the mean particle

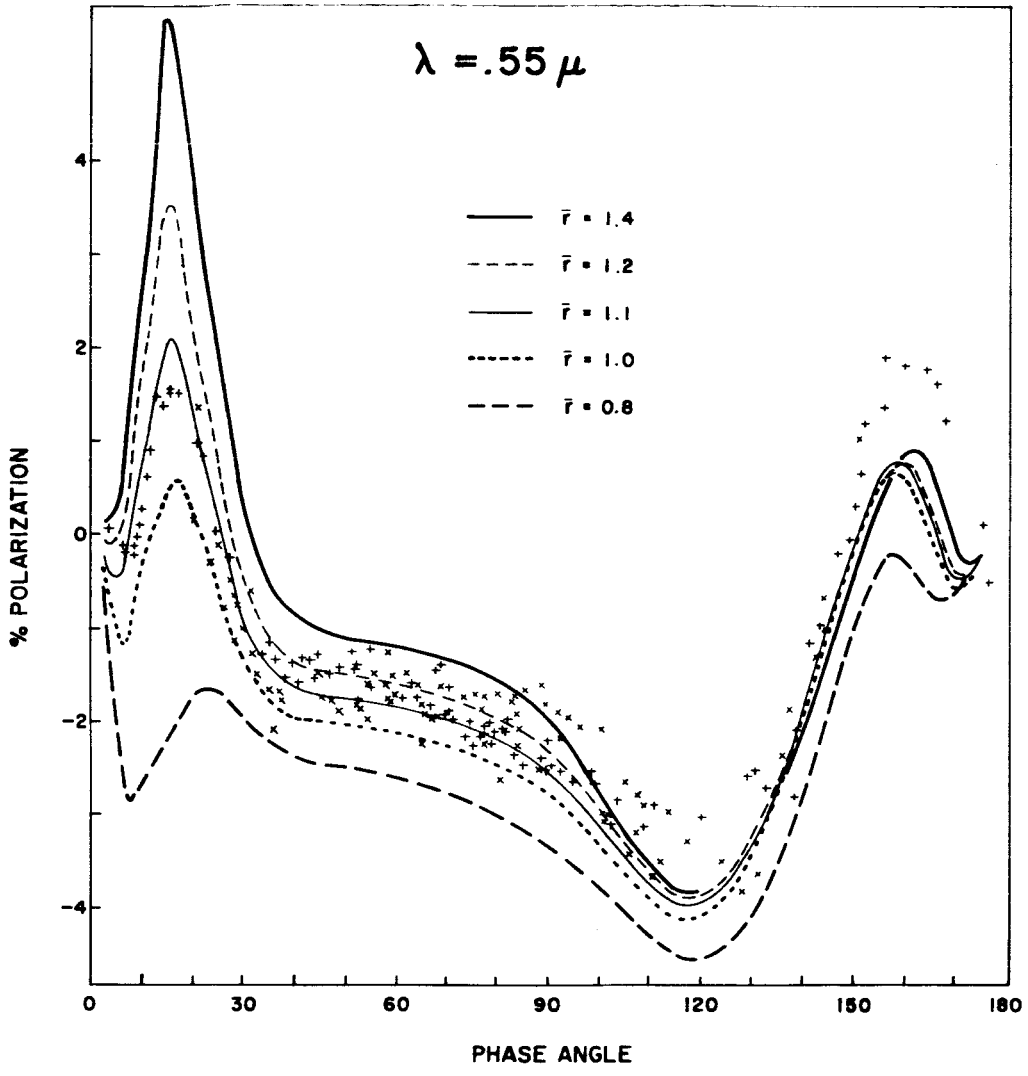

Fig. 20. The pluses represent the visual observations of Lyot, and the crosses are the intermediate-bandwidth observations of Coffeen and Gehrels at $\lambda = 0.55\mu$. The theoretical curves are for $n_r = 1.45$ with several values for the mean scattering radius $\bar{r}(\lambda=.55\mu)$. The albedo of Venus is assumed to be 87 percent, and the Rayleigh scattering determined in the ultraviolet region ($f_R = 0.045$) is included after reduction by a λ^{-4} law.

radius is ~1.1μ. The agreement is closer with the intermediate-bandwidth observations of Coffeen and Gehrels than with the broad-bandwidth observations of Lyot; this result is not surprising since the calculations are for a single wavelength.

There is a discrepancy with the observations at phase angles ~160°. From Fig. 7 it is clear that there would be better agreement in that region if a somewhat narrower size distribution were used, and it is also obvious that other features would hardly be changed by the use of the narrower distribution. Hansen and Hovenier (1972) have varied b and found that a better fit occurs for b~.08. What is most significant is the fact that the feature would be entirely smoothed away if a broad distribution were used. And it is clear that the feature for Venus is the polarization "island" (anomalous diffraction) in the contour diagrams: for shorter wavelengths it becomes weaker and for longer wavelengths it disappears.

The best fit to all of the observations occurs with a refractive index which decreases from ~1.46 in the ultraviolet region to ~1.43 at $\lambda = 0.99\mu$; the uncertainty in n_r is 0.02 at each wavelength. The mean particle radius is ~1μ. Most of the particles must be spherical: the glory, rainbow and anomalous diffraction feature are predicted for spheres but they are not expected for irregular particles. The width of the size distribution is amazingly small. The value $v_{eff} \sim .08$ is smaller than for terrestrial

water clouds (for which v_{eff} is usually in the range .10 - .25, the smaller values occurring for fair weather clouds and the large ones for convective clouds) and terrestrial tropospheric hazes (for which v_{eff} ~.2 -.4). However, two different measurements (Mossop, 1965; Friend, 1966) of the size distribution of particles in the earth's stratosphere (Junge layer) yielded v_{eff} ~.05 -.06, and the particles appeared to be liquid; thus perhaps for liquid particles in a convectively stable part of the atmosphere it is reasonable to find a narrow size distribution. In any case the derived particle shape and the width of the size distribution together strongly suggest that the cloud particles on Venus are liquid.

It should be emphasized that the cloud properties derived from the polarization refer to the top part of the clouds. Intensity measurements, for example, of absorption lines, include information on deeper layers where the cloud particle properties may differ and the pressure is certainly greater. This must also be borne in mind when one considers the color and spectral reflectivity of Venus. Nevertheless, the "polarization clouds" must be equated with the "visible clouds" of Venus; the polarization clouds have a significant optical depth on a planet-wide basis.* The fact that these clouds have a substantial optical thickness high in the atmosphere, where $p \lesssim 50$mb, only makes them all the more interesting.

It should also be emphasized that the visible clouds are composed of particles with a single refractive index (note, for example, the sharp rainbow in the ultraviolet); they cannot be composed of a mixture such as dust and water. Indeed, there is only one type of particle contributing significantly to the polarication. It there were two or more cloud layers with different particles (differing in refractive index or particle size or particle shape) contributing to the polarization then the features due to each type of particle would be present; however, the only features in the observed polarization are those corresponding to the particles described above (n_r~ 1.44, etc.) and moreover all of the features predicted for such particles are present. However, the fact that one type of particle is responsible for the polarization does not mean that the atmosphere can be regarded as homogeneous for other purposes; observations of absorption lines, e.g., refer to a greater depth of the atmosphere, and there are some indications of vertical inhomogenieties in these observations.

The above results stringently narrow the list of possible materials composing the visible clouds of Venus; indeed, most of the materials that have been proposed may be ruled out. The polarization data are incompatible with solid particulates such as SiO_2, NaCl, NH_4Cl, and $FeCl_2$ on several grounds, including their refractive indices. The refractive indices for pure water (H_2O) and ice are much too small, whereas the refractive indices for H_g and H_g compounds are much too large. Of course, the polarization results do not rule out the possible existence of these materials in some cloud deck beneath the visible clouds.

HCl - H_2O is one of the more probable of the possibilities for the cloud particle composition which have been suggested in the literature. Lewis (1969, 1972), using observed abundances of the gases HCl and H_2O, predicted that cloud particles composed of an aqueous solution of hydrochloric acid (HCl - H_2O), with ~25% HCl by weight, should exist at the ~50mb level. The refractive index of HCl, ~1.42 (Lewis, 1972), may just barely be compatible with the polarization results.

H_2SO_4 - H_2O has recently been suggested for the cloud particle composition on Venus by a group at JPL (A. Young, private communication). It appears that a solution of sulfuric acid of the appropriate composition could have the observed refractive index and be liquid at the cloud top temperature. Sulfur is a major constituent in the particulate layer in the Earth's stratosphere (the Junge layer) which exists at the 50mb region. On photochemical grounds Lewis argues against sulfuric acid in the clouds of Venus, but the possibility at least warrants a close examination.

Carbon suboxide (C_3O_2) has also been proposed as a possible cloud particle material on Venus (Sinton, 1953) and it has a refractive index ~1.45. However the spectroscopic upper limit on the abundance of its vapor (Jenkins, et al., 1969; Kuiper, 1969) is a few orders of

---

*At an optical depth $\tau = 1$ the contrast for average observing conditions, $\mu = \mu_o = \frac{1}{2}$, is already reduced to e^{-4}. Thus $\tau = 1$ is approximately the depth to which we can 'see'.

magnitude less than the amount required in the stratosphere of Venus for equilibrium with the condensate of the monomer. The low polymers may provide an alternative, but there are so many unanswered questions about C_3O_2 (see,e.g., Hansen and Arking, 1971) that it appears to be an improbable possibility.

The nature of the clouds of Venus could be more accurately specified if the vertical distribution of the cloud particles were established. This could be obtained from measurements of the polarization at a high spatial resolution over the planet, as from a planetary orbiter. It is also highly desirable that measurements of the polarization be extended into the near-infrared. An accurate tracing of the refractive index in that region, where variations are probable, could serve to uniquely identify the cloud particle composition.

7. POTENTIAL APPLICATIONS ON MJS

The Mariner Jupiter-Saturn missions provide a unique opportunity for obtaining information on several planets and their environment from photopolarimetric observations. The major advantages on the MJS missions are the greatly increased phase angle coverage and the close-up views with the attendant improved spatial resolution. Observations from Earth are limited to small phase angles ($<12^o$ for Jupiter, $<6^o$ for Saturn) and this eliminates most of the potential applications for polarization measurements.

The information obtainable from photopolarimetry covers a range from the relatively simple mapping of cloud heights to the derivation of detailed characteristics of particle microstructure. In the latter extreme the amount of detail which can be extracted in a given instance will depend in part on what the actual situation is; for example, for a case in which the particles are very irregular in shape it will be difficult to establish more about the particle microstructure than the fact that the particles are irregular and of some specific size range.

Cloud heights and macrostructure. It is known that there are clouds on Jupiter and Saturn. These clouds must play a major role in the radiative processes in these planetary atmospheres, both in the absorption of solar radiation and in the emission of infrared thermal energy. A knowledge of the cloud structures is essential for establishing the total atmospheric structure. It is probable that the clouds also play a major role in the atmospheric dynamics and that they can serve as an indicator of patterns of atmospheric motion.

Thus it would be valuable to have measurements of the cloud heights as a function of location on the planets. This can be achieved from measurements of the wavelength dependence of the polarization. The sharp variation with wavelength of the cross-section for Rayleigh scattering allows the number of gas molecules in a vertical column above the clouds to be established from measurements at two wavelengths, at least one of which has a non-negligible Rayleigh optical thickness above the clouds ($\tau_{Ray} \gtrsim .01$) and at least one of which is sufficiently transparent for Rayleigh scattering ($\tau_{Ray} \lesssim .05$). The filters selected for the proposed photopolarimeter will allow the measurement of cloudtop heights between ~10mb and at least ~latm. With Earth-based observations, because of the small available range of phase angles for the outer planets, it is only possible to conclude that the equatorial clouds on Jupiter are much higher than the polar clouds. However, the larger phase angles and higher spatial resolution attainable on the MJS missions will allow a mapping of cloud heights on Jupiter and Saturn. It will also be possible to determine whether there are clouds above ~latm on Uranus and Neptune, and, if there are clouds, average cloud heights can be obtained.

The gross cloud structure can also be extracted from the polarization in the sense that a haze can be distinguished from a more optically dense cloud. The essential distinction here is the mean free photon path or the visibility. Rayleigh scattering observable in the polarization may arise from gas encountered within the top part of the 'cloud' by photons whose total number of scatterings is small, as well as from gas above the clouds. In the case of terrestrial condensation clouds the Rayleigh scattering within the clouds can be neglected, but, on the other hand, the 'clouds' on Venus appear to be a diffuse haze with a long mean free path. On Jupiter and Saturn it is possible that some of the clouds are actually a haze, or that there are hazy regions above clouds. These alternatives can be distinguished by polarization measurements of a given region from different directions of observation. Some similar information can be obtained from measurements of the intensity as a func-

tion of the zenith angle ('limb darkening'), particularly if the strength of absorption lines is measured, but the interpretation of intensity observations is more model-dependent because they represent an average over a greater range of atmospheric depth.

Particle sizes. The classification of particles according to whether their mean size is less than, on the order of, or larger than the wavelengths employed can be made in all cases, regardless of the particle shape. For cases in which the particles and their scattering behavior can be theoretically modeled it is possible to obtain more precise information on the particle size. For both approximate and precise particle sizing observations are required at a few (3-5) wavelengths spaced over the available wavelength interval. To provide data for accurate theoretical modeling requires observations at these wavelengths over as wide a range of phase angles as possible.

At least some of the clouds on Jupiter and Saturn may be cirrus-like with the particle composition NH_3, NH_4HS or something else. If the particles are crystals with a size $\gtrsim$10 times the wavelengths it will be possible to establish from the polarization that their size has that lower limit. However, the cloud or haze particles may well be smaller than this, and in such a case it will be possible to establish their mean size at least within a factor of two.

For the rings of Saturn the same possibilities for particle size discrimination exist as for the clouds and hazes in planetary atmospheres. There is also the possibility that one or more of the rings of Saturn is composed of boulders which could be covered with finer particles. This possibility can be distinguished, by means of the polarization, from the case of scattering by independent particles. If the rings are in fact made of large boulders with textured surfaces, the information obtainable from the polarization will be comparable to that which can be inferred for planetary surfaces; it will be possible to distinguish an icy surface from one similar to that of the moon and also to obtain some measure of the scale of the surface texture.

Dust particles in interplanetary space and in the vicinity of the planets can also be investigated by absolute photometry and polarimetry measurements. These particles are well-suited for this type of investigation because they are certainly independent scatterers and they probably have a mean size on the same order as the wavelengths of the photopolarimeter. The measurements should allow the determination of the spatial distribution of interplanetary particles as well as their size and optical properties as a function of distance from the sun.

Particle microstructure. Details of the particle microstructure in addition to the mean particle size, such as more information on the size distribution and the refractive index, shape and phase of the particles, can often be obtained from the photopolarimetric observations. These different aspects of the microstructure are interrelated and the knowledge which can be obtained depends on the actual situations encountered.

The most reliable information on the particle shape is provided by the polarization of the scattered light as a function of phase angle. If the particles are spherical the shape is revealed by specific features in the polarization. In this particular case the nature of these features and their variation with wavelength can also be used to accurately establish the particle refractive index and in some cases also the width of the size distribution. A spherical shape also makes it very probable that the phase of the particles is liquid.

Nonspherical particles are easily distinguishable from spheres. For most nonspherical particles larger than the wavelength the only noticeable features in the polarization arise from rays reflected or twice refracted by the particles; for independently scattering particles this gives rise to a positive polarization at most phase angles, but a negative polarization near the forward scattering direction. For specific crystalline shapes there are specific features in the polarization, such as the ice crystal halos, which can be used for particle identification. These features depend on the crystal shape and refractive index. For cases such as Jupiter and Saturn, in which the clouds are suspected to have some specific composition, these polarization features can be used to confirm or reject the composition in question.

REFERENCES

Blau, H.H., D.J. McCleese and D. Watson, 1970: Scattering by individual transparent spheres. Appl. Opt. 9, 2522-2528.

Bryant, H.C., and A.J. Cox, 1966: Mie theory and the glory. J. Opt. Soc. Amer., 56, 1527-1532.

Coffeen, D.L., 1969: Wavelength dependence of polarization. XVI. Atmosphere of Venus. Astron. J., 74, 446-460.

Coffeen, D.L., and T. Gehrels, 1969: Wavelength dependence of polarization. XV. Observations of Venus. Astron.J., 74, 433-445.

Coffeen, D.L., and J.E. Hansen, 1972: Polarization of near-infrared sunlight reflected by terrestrial clouds. to be submitted to J.Atmos. Sci.

COSPAR, 1972: Application of space techniques to some environmental problems. Report of Working Group 6 to the United Nations, 73 pp.

Diem, M., 1948: Messungen der Grosse von Wolkenelementen II. Meteor. Rund., 1, 261-273.

Dollfus, A., and D.L. Coffeen, 1970: Polarization of Venus. I. Disk observations, Astron. Astrophys., 8, 251-266.

Fahlen, T.S., and H.C. Bryant, 1968: Optical backscattering from single water droplets. J. Opt. Soc. Amer., 58, 304-310.

Friend, J.P., 1966: Properties of the stratospheric aerosol. Tellus, 18, 465-473.

Greenberg, J.M., N.E. Pederson and J.C. Pederson, 1961: Microwave analog to the scattering of light by nonspherical particles. J. Appl. Phys., 32, 233-242

Hansen, J.E., 1971a: Circular polarization of sunlight reflected by clouds. J. Atmos. Sci., 28, 1515-1516.

Hansen, J.E., 1971b: Multiple scattering of polarized light in planetary atmospheres. Part I. The doubling method. J. Atmos. Sci., 28, 120-125.

Hansen, J.E., 1971c: Multiple scattering of polarized light in planetary atmospheres. Part II. Sunlight reflected by terrestrial water clouds. J. Atmos. Sci., 28, 1400-1426.

Hansen, J.E., and A. Arking, 1971: Clouds of Venus: Evidence for their nature. Science, 171, 669-672.

Hansen, J.E., and D.L. Coffeen, 1972: Polarization of near-infrared sunlight reflected by terrestrial clouds. Amer. Meteor. Soc., Conf. on Atmos. Rad., 55-60.

Hansen, J.E., and J.W. Hovenier, 1972: Interpretation of the polarization of Venus. to be submitted to J. Atmos. Sci.

Hansen, J.E., and J.B. Pollack, 1970: Near-infrared light scattering by terrestrial clouds. J. Atmos. Sci., 27, 265-281.

Holland, A.C., and G. Gagne, 1970: The scattering of polarized light by polydisperse systems of irregular particles. Appl. Opt., 9, 1113-1121.

Jacobowitz, H., 1970: Emission, scattering and absorption of radiation in cirrus cloud layers. Ph.D. thesis, Dept. Meteor., M.I.T.

Jenkins, E.B., D.C. Morton and A.V. Sweigart, 1969: Rocket spectra of Venus and Jupiter from 2000 to 3000 Å. Astrophys. J., 157, 913-924.

Kattawar, G.W., G.N. Plass and C.N. Adams, 1971: Flux and polarization calculations of the radiation reflected from the clouds of Venus. Astrophys. J., 170, 371-386.

Kemp, J.C., R.D. Walstencroft and J.B. Swedland, 1971: Circular polarization: Jupiter and other planets. Nature, 232, 165-168.

Kerker, M., 1969: The Scattering of Light and other Electromagnetic Radiation. New York, Academic Press, 666 pp.

Kuiper, G.P., 1969: Commun. Lunar Planet. Lab. 101, 1.

Lewis, J.S., 1969: Geochemistry of the volatile elements on Venus. Icarus, 11, 367-385.

Lewis, J.S., 1971: Refractive index of aqueous HCl solutions and the composition of the Venus clouds. Nature, 230, 295-296.

Liou, K.N., 1972a: Electromagnetic scattering by arbitrarily oriented ice cylinders. Appl. Opt., 11, 667-674.

Liou, K.N., 1972b: Light scattering by ice clouds in the visible and infrared: A theoretical study. J. Atmos. Sci., 29, 524-536.

Liou, K.N., and J.E. Hansen, 1971: Intensity and polarization for single scattering by polydisperse spheres. A comparison of ray optics and Mie theory. J. Atmos. Sci., 28, 995-1004.

Lyot, B., 1929: Recherches sur la polarization de la lumiere des planetes et de quelques substances terrestres. Ann. Obs. Paris (Meudon), 8, 161 pp.

Mossop, S.C., 1965: Stratospheric particles at 20 km altitude. Geochim. et cosmochim. Acta, 29, 201.

NASA, 1971: Remore measurement of pollution. NASA SP-285, 253 pp.

Pritchard, B.S. and W.G. Elliot, 1960: Two instruments for atmospheric optics measurements. J. Opt. Soc. Amer., 50, 191-202.

Sinton, W.M., 1953: thesis, Johns Hopkins University.

van de Hulst, H.C., 1957: Light Scattering by Small Particles. New York, Wiley, 470 pp.

van de Hulst, H.C., and K. Grossman, 1968: in The Atmospheres of Venus and Mars, ed. J.C. Brandt and M.B. McElroy (New York: Gordon and Breach), pp. 35-55.

Vinnichenko, N.K., 1972: presented to COSPAR Working Group VI, February 14-18, Boston.

Yeh, C., 1964: Scattering of obliquely incident light waves by elliptical fibers. J. Opt. Soc. Amer., 54, 1227-1231.